A tale of two signals: Global and local influences on the Late Pleistocene loess sequences in Bulgarian Lower Danube

Fenn, Kaja[a,b]*, Thomas, David S.G.[b], Durcan, Julie A.[b], Millar, Ian L.[c], Veres, Daniel[d], Piermattei, Alma[e], Lane, Christine S.[e]

[a] Department of Geography and Planning, University of Liverpool, Liverpool L69 7ZT

[b] Oxford University Centre for the Environment, South Parks Road, Oxford OX1 3QY, UK

[c] Geochronology and Tracers Facility, British Geological Survey, Keyworth, Nottingham NG12 5GG, UK

[d] Romanian Academy, Institute of Speleology, Clinicilor 5, 400006, Cluj-Napoca, Romania

[e] Department of Geography, University of Cambridge, CB2 3EN, UK

* Corresponding author: Kaja.Fenn@liverpool.ac.uk

Highlights

- Over short distances local factors including topography and proximity to mountain belts influenced loess profile variability.
- Provenance and chronological results show a minor switch in the sediment delivery mode and/or source between MIS2 and MIS3.
- The most northerly terrestrial site containing the Cape Riva/Y2 tephra provides a new tephra marker for Danubian loess.
- First application of single grain zircon U–Pb dating as a tool for understanding depositional history of Lower Danube loess.

Abstract

In Central and Eastern Europe, research has been focused on loess associated with a plateau-setting, which preserves distinct and well-developed loess and palaeosol units linked to orbital scale changes. This has led to the view that during the last glacial period the Middle and Lower Danube predominantly experienced dry continental climates and supported steppic environments. However outside of the typical plateau setting, some authors have reported a presence of embryonic palaeosols within loess units suggesting sufficient moisture for short-term pedogenesis, and therefore either large scale moisture delivery systems and/or influence of local climatic and/geomorphic factors. Here the palaeoenvironmental and palaeoclimatic history is reconstructed based on two loess-palaeosol profiles in Slivata, North Bulgaria. The site is located in proximity to both the Carpathian and Balkan Mountains and rest on the Danube river terrace. To understand the timing of sediment deposition and dust fluxes chronological approaches combining quartz optically stimulated luminescence (OSL), feldspar post infrared-infrared stimulated luminescence (pIR-IRSL), and tephra correlation were applied. The results are coupled with high-resolution particle size and magnetic susceptibility analysis to provide an overview of past environmental conditions at the site. Finally, zircon U-Pb ages are used to understand potential changes to sediment delivery patterns, in the context of the site development.

The investigated profile at Slivata 2 preserves a loess-palaeosol record spanning 52-30 ka, with a very complex sedimentary sequence that switches between periods of enhanced dust flux and sediment accumulation, and palaeosol development. The Slivata 2 sequence is also punctuated by multiple thin “palaeosol” like units that are interpreted as colluvial “soil” deposits on the basis of sedimentology, provenance, and geochronology, indicating a highly variable and dynamic landscape responding to the surrounding environment. The chronology shows very rapid sediment accumulation at Slivata 1 during LGM, with mass accumulation rates similar to sites in the Carpathian Basin, suggesting strong winds and high sediment supply rates. Yet LGM loess is punctuated by a thin palaeosol, which developed between 20-19 ka. This coincides with a temporary glacial retreat in the Carpathian Mountains and higher moisture availability in Eastern Carpathians, and therefore points to localised influences on loess-palaeosol development. Moreover data from Slivata 1 shows soil development and by extension landscape and climate stabilisation shortly prior to 14 ka. The pre-Holocene onset of pedogenesis at Slivata supports ecological and glacial evidence of weak Younger Dryas from the South Carpathian Mountains.

Lastly this paper provides a geochemical analysis of the thin tephra horizon preserved in the Slivata 2 profile, which was correlated to the Cape Riva/Y-2 tephra. Consequently Slivata is the most northerly terrestrial site found to contain this tephra horizon, which has implications for the understanding of the size of the Santorini’s Cape-Riva/Y-2 explosion. The identification of the Cape Riva (Y-2) tephra horizon and new remodelled age of 21.92±0.56 cal ka BP provides a new tephrostratigraphic marker for eastern European LGM loess.

Keywords

Luminescence (OSL), Cape Riva (Y2) tephra, Provenance, U-Pb dating, Quaternary, palaeoclimate, zircon, paleoenvironment

1. Introduction

1.1. The role of global, regional, and local controls on loess formation

Loess-palaeosol sequences (LPS) are one of the key long-term terrestrial archives preserving local, regional, and global palaeoclimate signals over timescales from 10^2 – 10^6 years (Fenn and Prud'Homme, 2020; Fitzsimmons et al., 2012; Marković et al., 2009; Muhs, 2013; Stevens et al., 2020). Due to their extensive spatial distribution they provide palaeoclimatic insights into regions where other archives are rare and often temporally limited, and allow for investigation of long-term environmental changes (Antoine et al., 2009b; Fenn et al., 2020a; Marković et al., 2007; Moine et al., 2017; Schatz et al., 2011; Újvári et al., 2017; Zech et al., 2013), landscape evolution (Kehl et al., 2021; Wolf et al., 2021), mechanisms of dust emission (Albani et al., 2015; Sima et al., 2009; Stevens et al., 2013; Újvári et al., 2013), and variability in dust flux (Fenn et al., 2020b; Mahowald et al., 2006; Újvári et al., 2010).

During the last glacial period the Danube region is thought to have predominantly experienced mostly steppic, continental climates (Marković et al., 2018b; Zech et al., 2013), with conditions too dry to sustain short-term pedogenesis (Marković et al., 2015). This resulted in "classic" loess profiles, comprising thick glacial loess units, separated by well-developed interglacial palaeosols and, at some sites, weakly developed interstadial palaeosols (Buggle et al., 2009; Fitzsimmons and Hambach, 2014; Fuchs et al., 2008; Marković et al., 2009; Vasiliniuc et al., 2011). These classic loess-palaeosol sequences are typically located in a plateau setting and can be linked to large-scale, orbitally driven climate changes (Zeeden et al., 2018b). Their relatively straightforward stratigraphy, spatial continuity, and widespread exposure led to extensive investigations and attempts to establish a unified long-term regional chronostratigraphic model for the Danube loess (Lehmkuhl et al., 2021; Marković et al., 2015).

Some loess-palaeosol sequences, especially in Western Europe, preserve evidence of short-term pedogenesis (i.e. embryonic palaeosols) within glacial loess units (Antoine et al., 2003, 2001; Haesaerts et al., 2016; Meszner et al., 2013), which does not fit with the "classic" orbitally driven loess-palaeosol sequences. The palaeosol development and pedogenetic intensity have been linked to millennial-scale variability and availability of moist, oceanic air from the North Atlantic (Antoine et al., 2001; Rousseau et al., 2017; Terhorst et al., 2015). The penetration of an oceanic influence on northern and eastern sections of the Danubian loess is thought to have caused more humid conditions that resulted in palaeosol and palaeosol-like horizons in the glacial units in, for example, Austria (Terhorst et al., 2015, 2014), Czech Republic (Antoine et al., 2013; Hošek et al., 2015), Poland (Jary and Ciszek, 2013), and even Ukraine (Rousseau et al., 2011; Veres et al., 2018).

Further a deviation from the classic loess-palaeosol stratigraphy was noted for some southern sites e.g. Nosak (Marković et al., 2014a; Perić et al., 2020) and Stalać (Bösken et al., 2017; Obreht et al., 2016) (Figure 1). These non-plateau setting sites preserve embryonic and fairly well-developed pedogenic horizons within major loess units, indicating that either moist air from the Atlantic penetrated further into the continent or that local climatic and/or geomorphic factors strongly influence individual sites. However some loess profiles from the Lower Danube (Obreht et al., 2017), alongside Dim cave speleothem record (Ünal-İmer et al., 2015), indicate that during the last glacial period the growing Fennoscandian Ice-Sheet and strengthening Siberian High blocked continental penetration of moisture-bearing North Atlantic air (Cohen et al., 2001; Rimbu et al., 2014; Schaffernicht et al., 2020) and shifted the jet-stream and westerly winds southwards. Therefore making significant moisture penetration alone an unlikely agent behind pedogenic horizon development in the Central European and Danubian loess. Given climate is only one of the factors that control pedogenesis, there is a need to investigate and consider the role of site-specific factors in loess profile development such as palaeotopography, sediment availability, presence of vegetation, and local microclimatic.

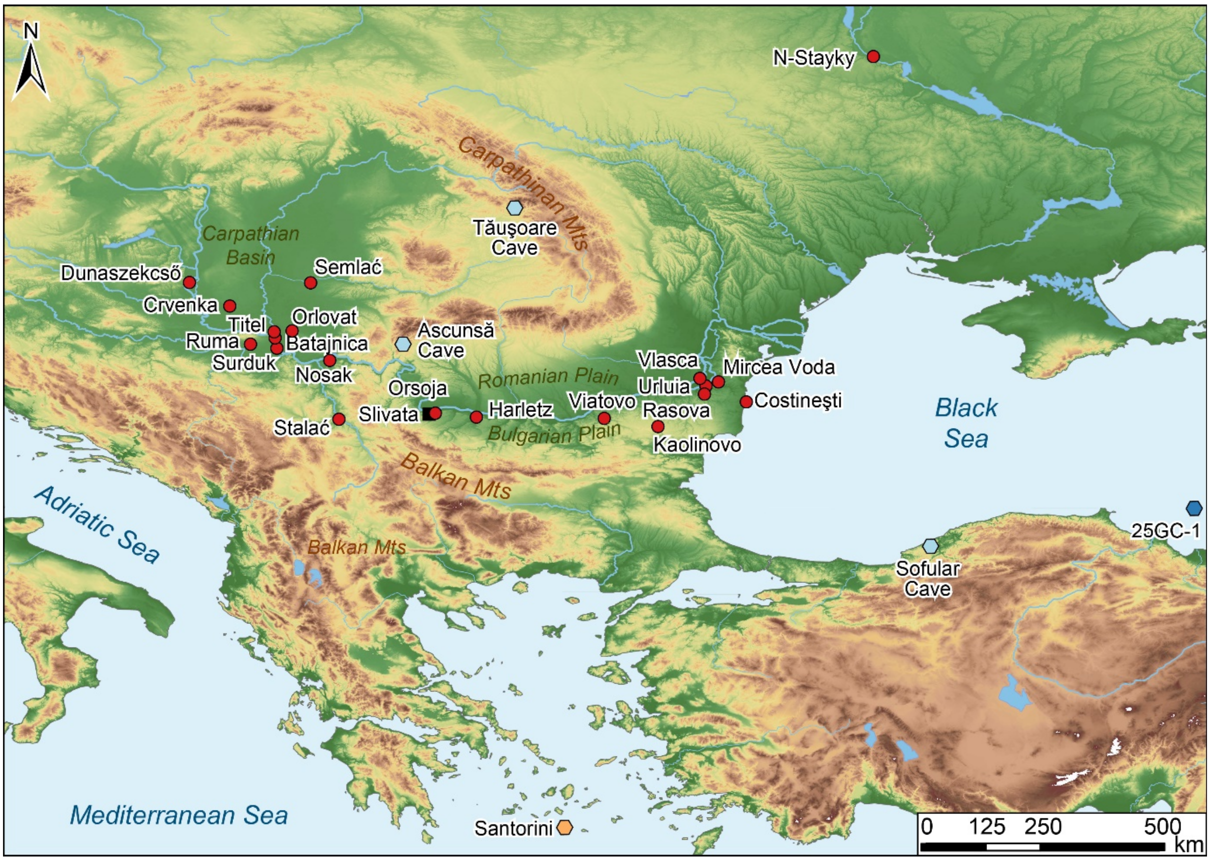

1.2. Loess chronology

Pedostratigraphic variability, alongside trends in magnetic susceptibility (Marković et al., 2012, 2008) and grain size (Antoine et al., 2009a) have been widely used to provide chronological controls for LPS (Zeeden et al., 2018c). These approaches inevitably make assumptions regarding the continuity of deposition or that magnetic susceptibility shifts reflect geochronological synchroneity, both of which have been challenged since these approaches were employed (Fenn et al., 2020b; Stevens et al., 2018, 2008). To address questions of global versus regional controls on LPS variation, and the idea of synchronous depositional and pedogenic response of LPS across the Middle and Lower Danube, a robust and absolute chronology is critical. Optically Stimulated Luminescence (OSL) dating has become the approach of choice within loess research as the method estimates the time of deposition of sediment and can provide chronologies for the whole glacial-interglacial cycle. OSL has been widely applied to Danubian loess sequences including Bulgaria (Balescu et al., 2020; Lomax et al., 2018), Croatia (Fenn et al., 2020a; Wacha and Frechen, 2011), Hungary (Novothny et al., 2011, 2002; Újvári et al., 2014a), Serbia (Avram et al., 2020; Fenn et al., 2020b; Murray et al., 2014; Perić et al., 2019, 2020; Stevens et al., 2011), and Romania (Constantin et al., 2014; Fitzsimmons and Hambach, 2014; Vasiliniuc et al., 2011). However, not all studies use high-resolution absolute dating approaches or combine multiple chronological approaches (see Scheidt et al., 2021), limiting their effectiveness for comparing records between loess profiles and with other archives.

1.3. Study aims

The Quaternary history of the Danube's LPS in proximity to the Iron Gorge is still relatively poorly understood, with the closest profiles located in Nosak (Marković et al., 2014a; Perić et al., 2020), Orsoja (Avramov et al., 2006), and Harletz (Antoine et al., 2019; Avramov et al., 2006; Lomax et al., 2018). Therefore, the potential modifying and long-term effect of the Carpathian and Balkan Mountains on the regional hydroclimate has not been fully explored (Longman et al., 2019). This study attempts to address this question by providing a detailed multi-proxy investigation of two LPS near Slivata village, northern Bulgaria (Figure 1). This Slivata site was selected to address the paucity of data for LPS sites in the Iron Gorge region of the Danube (Figure 1), and to provide an opportunity for palaeoenvironmental reconstruction which could be used as a context for sediment source analyses within a larger provenance research project (Fenn, 2019). Slivata loess contains numerous palaeosol horizons but also thin loess units and therefore appears stratigraphically distinctive from many late Quaternary LPS in the Lower Danube (Balescu et al., 2010; Fitzsimmons and Hambach, 2014; Lomax et al., 2018; Zeeden et al., 2018c) or the Carpathian Basin (Fuchs et al., 2008;

Stevens et al., 2011; Újvári et al., 2014a). Here results of single-grain detrital zircon U-Pb dating are combined with sedimentological analyses supported by 17 luminescence ages and tephrochronology to help understand and link the complex sedimentary histories of the investigated sites. In doing so, this study contributes to the ongoing debates regarding global versus regional/local controls on loess profile development, and to developments in loess sequence chronological control.

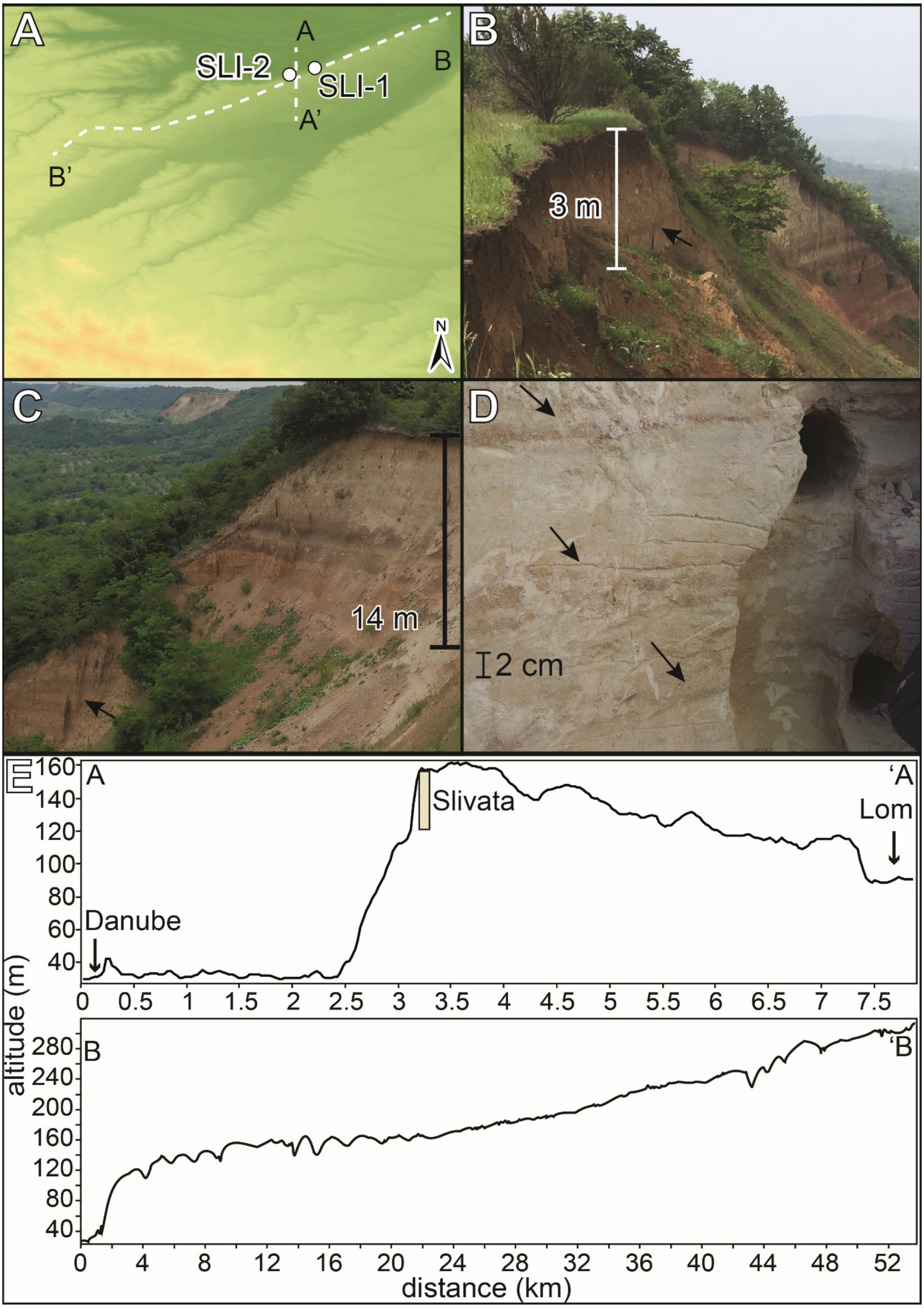

Figure 2. A) Area map showing the relative locations of the two Slivata profiles as well as the position of the two topographic cross sections (DEM Source: ©JAXA); B) Slivata 1 loess-

palaeosol profile. A faint brown horizon (marked by the black arrow) towards the bottom of the marked 3 m part of the section is Unit IV; C) Slivata loess-palaeosol 2 profile. Welded palaeosols (marked by the black arrow) are visible extending to the bottom of the section. Slivata 1 exposure is visible in the background; D) Thin reddish "palaeosol-like" bands described at the Slivata 2 profile (see Figure 3); E) Topographic cross sections: A-'A from the Danube's channel to the Lom River (N-S), and B-B' from Lom to along the plateau to Oreshets (NE-SW).

2. Study area and description

The study area is located in the piedmont of the Balkan and Carpathian Mountains before the Danube's valley widens into the Romanian Plain (Figure 1). The area experiences a Cfa climate; humid warm temperate with hot summers (Kottek et al., 2006), mean annual temperature of 11.6°C, and mean annual precipitation of 543 mm. Maximum rainfall occurs in June (67 mm/month), with August on average the driest month (34 mm/month). It belongs to cool temperate subhumid forest steppe biome under the Holdridge's life zones system (Szelepcsényi et al., 2014), with predominantly luvisol, vertisol, and chernozem style soils (European Soils Bureau, 2005). The southern bank of the Danube River preserves between two and six Pleistocene to Pliocene river terraces (Evlogiev, 2007) on top of which thick LPS (15-30 m) that form small plateaus are preserved. The Quaternary activity of the Danube River and its tributaries has been an important influence on the region's geomorphology (Boengiu et al., 2011; Evlogiev, 2015) as it heavily incised the LPS, creating a sequence of ridges and gullies that extend in a SW-NE direction (Figure 2A).

From an extensive loess wall that extends between the Lom and Skomlya rivers, two sites separated by ~2 km were selected; Slivata 1 (SLI-1; 43°46'0.91"N, 23°04'48.49"E) and Slivata 2 (SLI-2; 43°45'45.44"N, 23°03'29.55"E). Both exposures are part of the loess cliff (~3 km from the modern Danube channel), which slopes gently southwards towards the Lom river channel (Figure 2E; cross section A-'A). These LPS are part of a narrow (~4.5 km), elongated, gently sloping plateau like feature (Figure 2A) in a NE direction (Figure 2E; cross section B-'B) shaped predominantly by the Lom and Danube rivers. The Slivata sequences are thought to rest on the fifth river terrace (T5), 25 m above the alluvial floodplain (Avramov et al., 2006; Evlogiev, 2000). Whilst development of a T0 alluvial plain is linked to modern day processes and T1 to the Holocene, the exact age of the T5 terrace is not known. The natural exposures reveal over 15 m of loess and loess like deposits (Figure 2 and Figure 3), underlain by a complex sequence of welded palaeosols (Figure 2C). The initial field assessment suggested that several stratigraphic units can be traced between the two sites.

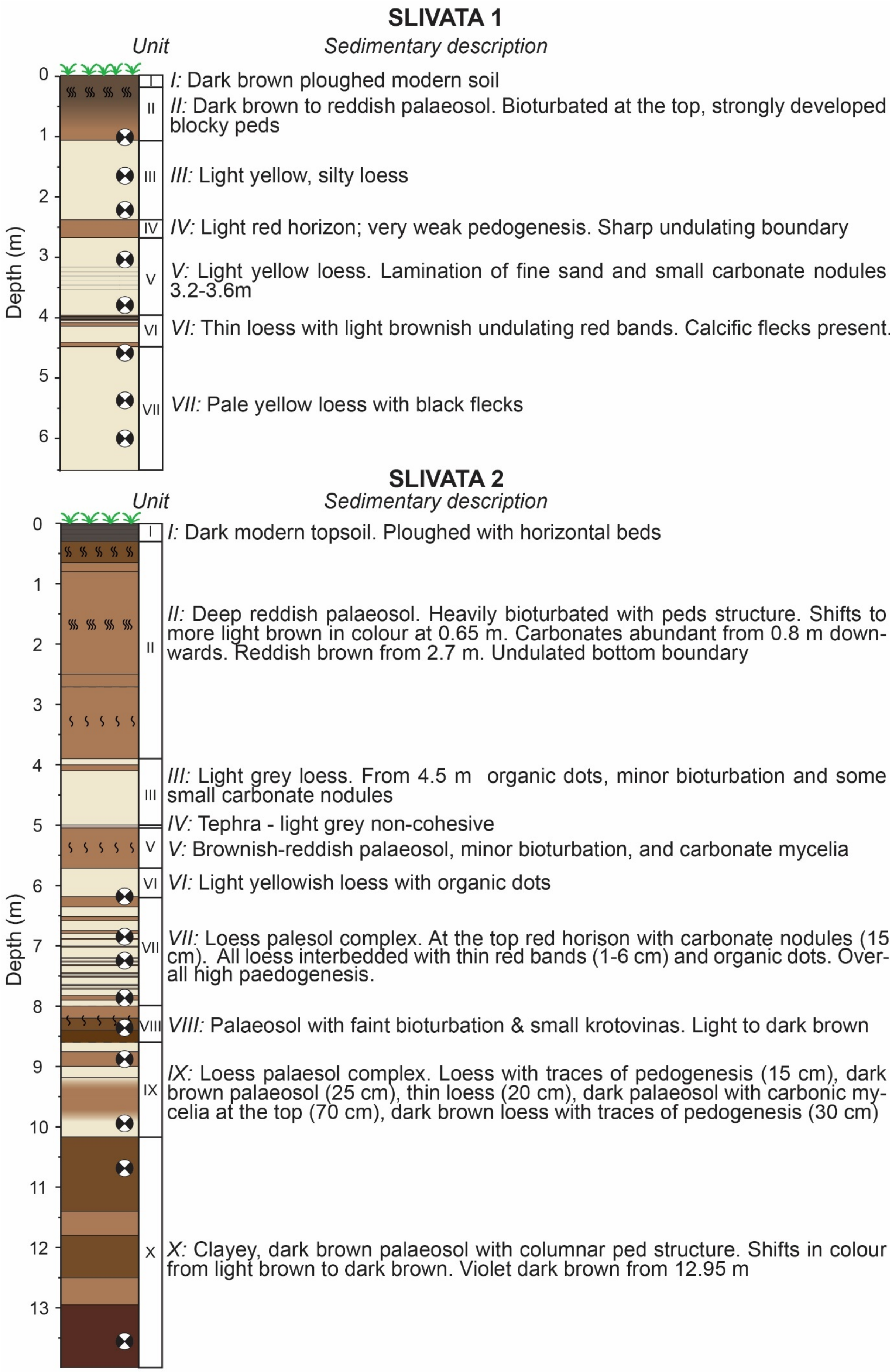
SLIVATA 1
Unit
Sedimentary description
Depth (m)
0
1
2
3
4
5
6
I
II
III
IV
V
VI
VII
I: Dark brown ploughed modern soil
II: Dark brown to reddish palaeosol. Bioturbated at the top, strongly developed blocky peds
III: Light yellow, silty loess
IV: Light red horizon; very weak pedogenesis. Sharp undulating boundary
V: Light yellow loess. Lamination of fine sand and small carbonate nodules 3.2-3.6m
VI: Thin loess with light brownish undulating red bands. Calcific flecks present.
VII: Pale yellow loess with black flecks
SLIVATA 2
Unit
Sedimentary description
Depth (m)
0
1
2
3
4
5
6
7
8
9
10
11
12
13
I
II
III
IV
V
VI
VII
VIII
IX
X
I: Dark modern topsoil. Ploughed with horizontal beds
II: Deep reddish palaeosol. Heavily bioturbated with peds structure. Shifts to more light brown in colour at 0.65 m. Carbonates abundant from 0.8 m downwards. Reddish brown from 2.7 m. Undulated bottom boundary
III: Light grey loess. From 4.5 m organic dots, minor bioturbation and some small carbonate nodules
IV: Tephra - light grey non-cohesive
V: Brownish-reddish palaeosol, minor bioturbation, and carbonate mycelia
VI: Light yellowish loess with organic dots
VII: Loess palesol complex. At the top red horison with carbonate nodules (15 cm). All loess interbedded with thin red bands (1-6 cm) and organic dots. Overall high paedogenesis.
VIII: Palaeosol with faint bioturbation & small krotovinas. Light to dark brown
IX: Loess palaesol complex. Loess with traces of pedogenesis (15 cm), dark brown palaeosol (25 cm), thin loess (20 cm), dark palaeosol with carbonic mycelia at the top (70 cm), dark brown loess with traces of pedogenesis (30 cm)
X: Clayey, dark brown palaeosol with columnar ped structure. Shifts in colour from light brown to dark brown. Violet dark brown from 12.95 m

Figure 3. Schematic stratigraphy for both Slivata loess-palaeosol profiles including sedimentological descriptions based on field observations. Position of the luminescence samples is marked by the circles.

3. Methods and materials

3.1. Sample collection

Section details, sedimentary descriptions, and age sampling locations are shown in Figures 2 and 3. Both sections were logged in detail in the field prior to sampling for dating and sedimentary analyses. For sedimentological analyses, 527 samples were collected contiguously at a 2 cm resolution; at Slivata 1 that represents the top 6 m of the profile and at Slivata 2 the middle ~4.5 m (Figure 3). For luminescence dating 17 samples were collected, ~50 cm apart by hammering opaque, light-tight plastic tubes into the freshly cleaned profiles. Additionally, at the depth of each luminescence sample, 1-2 kg of sediment was collected for provenance analysis (Fenn, 2019). Finally, a sample for geochemical analysis was collected from a thin, but visible, tephra horizon at 5 m of Slivata 2.

3.2. Sedimentological analysis

Following overnight sample drying and homogenisation, grain-size was analysed using a Malvern Mastersizer Hydro 2000MU laser diffraction particle size analyser. Chemical treatment of samples prior to analysis proved to be unnecessary (Supplementary Materials Figure S1) and therefore samples were measured without pre-treatment. Distribution data was converted to particle size classes, with all classes presented. Additionally, to investigate wind strength and broader scale aeolian dynamics, a U-ratio was determined (Vandenberghe and Nugteren, 2001). The U-ratio excludes pedogenic components formed *in situ* and grains transported over very short distances (sand) and was calculated as a ratio between fine and medium silt (% of 16–44 μm fractions to % of 5.5–16 μm fractions).

To determine the strength of pedogenesis magnetic susceptibility (χ) was investigated using a Bartington MS2 Magnetic Susceptibility System with a MS2B dual frequency sensor. Following the established protocol (Buggle et al., 2014; Gocke et al., 2014), prior to analysis samples were oven dried (max. 40° C), gently disaggregated, and packed into 10 cm^3 plastic cylindrical containers. Each sample was measured six times both at low (χ_{lf}) and high (χ_{hf}) frequencies, 0.465 kHz and 4.65 kHz respectively, and the mean value of the six analyses used to calculate mass-specific magnetic susceptibility (m^3 kg^{-1}). A standard sample of known magnetic susceptibility value was measured periodically (approximately every ten samples) to test for instrument drift. Frequency-dependent magnetic susceptibility (χfd) can provide an indication of the changes in concentration of ultra-fine superparamagnetic material, that is pedogenic in origin (Buggle et al., 2014; Schaetzl et al., 2018). The frequency dependence in absolute values (Δχ) presented in 10^{-8} m^3 kg^{-1} was determined as

$$\Delta\chi = \chi_{lf} - \chi_{hf}$$

and χfd (%) was calculated as:

$$\chi fd(\%) = ((\chi_{lf} - \chi_{hf})/\chi_{lf}))\ x\ 100$$

3.3. Geochronology

3.3.1. Tephra

A standard non-destructive tephra extraction method (Blockley et al., 2005) was followed to concentrate glass shards. The sample was treated with 7% HCl to remove carbonates, wet sieved (>25 µm), and density separated (1.95-2.55 g cm^{-3}). Finally, isolated shards were mounted on epoxy resin stubs, and polished to expose their surfaces ready for shard-specific compositional analysis by electron microprobe.

To determine concentrations of major and minor element oxides within glass shards, samples were analysed using a Cameca SX100 wavelength dispersive electron microprobe analyser (WDS-EPMA) in the Department of Earth Sciences, University of Cambridge. A 10 µm diameter defocused beam spot operating at 15 kV and 6 nA was used. Counts for sodium were collected over 10 second acquisitions, chlorine and phosphorus for 60 seconds and all other elements for 30 seconds. Secondary standards including a range of MPI-DING (Jochum et al., 2006) fused volcanic glasses were periodically measured to monitor analytical precision and accuracy (see Supplementary Materials Table S1 for details).

Data reduction involved the removal of three analyses that erroneously targeted non-tephra grains, and three individual glass shard analyses with element oxide analytical totals below 94 weight %. The remaining compositional data (n=43) were normalised to anhydrous basis for comparison to reference datasets (Table 1, Figure 4) (Supplementary Materials Table S2).

Table 1. Mean values for major and minor element oxide concentrations (as normalized weight %) of glass shards from Slivata. See Table S2 for details of individual shard analysis and Table S1 for raw, unnormalized data.

SLV_T5	SiO_2	TiO_2	Al_2O_3	FeO	MnO	MgO	CaO	Na_2O	K_2O	P_2O_5	Total
Mean	72.62	0.46	14.29	3.13	0.12	0.42	1.72	4.09	3.08	0.08	100
2σ	0.51	0.03	0.33	0.20	0.08	0.03	0.09	0.45	0.17	0.06	

3.3.2. Luminescence dating

Samples for luminescence dating were opened and prepared under subdued orange light conditions at the Oxford Luminescence Dating Laboratory. The exposed material from the end of the sampling tube was retained for dose rate analysis. Bulk sediment was treated with HCl and H_2O_2 to remove carbonates and organic matter. The 4-11 μm and 63-90 μm fractions were isolated through a combination of sieving and settling. Coarse-grained potassium feldspar was obtained through density separation, while quartz enriched fine-grained sediment was treated with H_2SiF_6 to remove non-quartz minerals. 4-11 μm quartz grains were dispensed onto the surface of 9.8 mm aluminium discs, whereas for 63-90 μm K-feldspar small aliquots (2 mm in diameter) were used. Full details of sediment preparation, measurement conditions, and analysis for quartz and feldspar protocol determination are provided in the supporting information (Supplementary Materials Figures S2, S3, and S4, and Tables S2 and S3).

All measurements were carried out using Risø TL/OSL luminescence readers fitted with a calibrated $^{90}Sr/^{90}Y$ beta source and a bialkali photomultiplier tube. Quartz grains were stimulated with blue-light emitting diodes (470 nm) and the signal was measured in a UV detection window through 7.5 mm U-340 glass filters (Bøtter-Jensen et al., 2000). K-feldspars were stimulated with infra-red emitting diodes (870 nm), and the signal was detected in the blue-violet region through a combination of Schott BG39/Corning 7-59 filters. The single aliquot regenerative (SAR) dose protocol (Murray and Wintle, 2000; Wintle and Murray, 2006) was used for equivalent dose determinations. Prior to final D_e calculation, all luminescence signals were screened using standard rejection criteria, i.e. signal recuperation (<5%), recycling ratio (Murray and Wintle, 2000), and in the case of quartz, OSL IR depletion ratios (Duller, 2003) which were set at 1±10%. Given the low overdispersion (between 0% and 9.9%) of dose distributions, D_es were calculated using the central age model (CAM; Galbraith et al., 1999).

Concentrations of uranium, thorium, potassium and rubidium were measured by inductively coupled plasma mass spectrometry at British Geological Survey, Keyworth (BGS) to determine environmental dose rates. Radionuclide concentrations were converted to infinite-matrix dose rates using the conversion factors of Guérin et al., (2011) and a moisture content of 15±5%, which is typically used for loess sediments (Schatz et al., 2012; Stevens et al., 2011; Újvári et al., 2014a). Dose rate calculations were carried out using the DRAC (v1.2) software (Durcan et al., 2015). The results are presented in Table 2.

3.3.3. Age-depth modelling and Mass Accumulation Rates (MARs)

To better visualise the age distributions, age-depth models for both Slivata profiles were developed based on the luminescence ages and further constrained through tephrochronology (Supplementary Materials Figures S5 and S6). Although some age-depth modelling software can incorporate luminescence data, e.g. Bacon (Blaauw and Christeny, 2011) or OxCal (Bronk Ramsey, 1995), they were created for radiocarbon age calibration and modelling, and therefore do not capture fully the complexities of luminescence age errors.

The recently developed Zeeden et al. (2018a) ADmin script uses a composite of an inverse modelling and a Bayesian age-depth model to refine luminescence ages. It creates separate probability density functions for systematic and random uncertainties, but utilises only the random uncertainty to recalculate the uncertainties. All luminescence ages were modelled using this approach, and all subsequently ages mentioned in the text refer to the modelled results (Figures 5 and 7).

To place Slivata in the context of the region's palaeoclimatic and environmental data, a comparison between other loess profiles was necessary. Sites for comparison were chosen based on stratigraphy, relatively high-resolution absolute chronology, and the availability of proxy data. To ensure consistency between Slivata and loess profiles selected from the literature all chronologies were first modelled using ADmin script (Zeeden et al., 2018a). Age change with depth was analysed to ensure no major hiatuses were present. This was the case for all sites apart from Orlovat (Marković et al., 2014b) where a large part of MIS2 loess is thought to be missing. Nonetheless data from Orlovat was still used, although caution was taken when interpreting of the MIS 2 period. The re-modelled OSL ages for each site formed a basis for the development of past dust fluxes estimates, Mass Accumulation Rates (MARs). MARs were calculate following the Kohfeld and Harrison (2003) equation:

$$MAR\ (g\ m^{-2}\ a^{-1}) = SR\ x\ f_{eol}\ x\ \rho_{dry}$$

where SR is sedimentation rate (m a^{-1}), f_{eol} is the fraction of the sediment that is aeolian, and ρ_{dry} is dry bulk density (g cm^{-3}). As loess is primarily aeolian in origin f_{eol} is assumed to be 1. An estimated bulk density value of 1.5 g cm^{-3} was used based on the typical loess values from the region (Fenn et al., 2020a; Perić et al., 2019; Újvári et al., 2010). The same bulk density values were used in DRAC and MAR calculations. To take into consideration the age uncertainty for all sites, MAR_{min} and MAR_{mean} were calculated following suggestions in Fenn et al. (2020a). Whilst it is difficult to assign a likelihood of an individual MAR, the investigation of minimum and average rates of deposition allows for testing of broad temporal trends. Finally, to plot loess proxy data on a continuous-age depth scale and provide a basis for comparison, modelled luminescence ages were used to interpolate ages at the resolution of the proxy data at each site using Bacon script (Blaauw and Christeny, 2011).

Table 2. Radionuclide concentrations, dose rates, D_e values and final luminescence ages for the 4-11 µm quartz and 63-90 µm K-feldspars. Infinite matrix dose rates were calculated using the conversion factors of Guérin et al. (2011) and adjusted for alpha efficiency (0.04±0.004 for 4-11 µm quartz (Rees-Jones, 1995), and 0.15±0.05 for coarse K-feldspars (Balescu and Lamothe, 1994)), grain size (alpha (Brennan et al., 1991) and beta (Mejdahl, 1979)), and a moisture content of 15±5%. For the K-Feldspar sample, an internal K concentration of 12.5±0.5% (Huntley and Baril, 1997) was used to calculated the internal dose rate. Cosmic dose rates were calculated according to Prescott and Hutton (1994). All calculations were made prior to rounding. Modelled ages were calculated using the ADmin script (Zeeden et al., 2018a) script and are used in the discussion. *m–measured, a–accepted, OD-Overdispersion.

Sample	Depth (m)	Mineral	Aliquots (m/a)*	U (ppm±1σ)	Th (ppm±1σ)	K (%±1σ)	Cosmic (Gy ka^{-1}±1σ)	Total dose rate (Gy/ka)	OD (%)*	De (Gy)	Age (ka)	Modelled age (ka)
BUL17/1/1	1.00	Quartz	15/15	1.45±0.15	8.94±0.89	1.48±0.15	0.19±0.02	2.70±0.18	5.4	38.06±0.68	14.11±1.00	14.11±1.07
BUL17/1/2	1.65	Quartz	15/15	1.48±0.15	8.19±0.82	1.20±0.12	0.17±0.02	2.37±0.16	3.2	46.36±0.60	19.53±1.36	18.88±1.05
BUL17/1/3	2.35	Quartz	15/15	1.68±0.17	8.63±0.86	1.41±0.14	0.16±0.02	2.65±0.18	6.6	51.20±1.10	19.32±1.38	19.57±1.07
BUL17/1/5	3.10	Quartz	15/15	1.58±0.16	8.62±0.86	1.40±0.14	0.15±0.02	2.60±0.18	2.8	53.40±0.90	20.57±1.45	20.53±1.06
BUL17/1/7	3.90	Quartz	15/15	1.73±0.17	8.82±0.88	1.22±0.12	0.13±0.01	2.48±0.17	9.9	54.00±1.80	21.80±1.68	21.40±1.08
BUL17/1/9	4.55	Quartz	15/15	1.76±0.18	8.86±0.89	1.28±0.12	0.12±0.01	2.53±0.18	0.0	56.30±0.90	22.22±1.60	22.04±1.05
BUL17/1/11	5.55	Quartz	15/15	1.83±0.18	9.13±0.91	1.17±0.12	0.11±0.01	2.47±0.18	7.3	55.77±0.87	22.61±1.65	22.66±1.21
BUL17/1/12	6.00	Quartz	15/14	1.68±0.17	7.92±0.79	1.36±0.14	0.11±0.01	2.48±0.17	6.0	54.87±1.28	22.09±1.63	23.30±1.50
BUL17/2/12	6.36	Quartz	15/14	1.81±0.18	8.40±0.84	1.22±0.12	0.10±0.01	2.44±0.17	4.6	72.15±3.93	30.85±2.26	30.04±1.70
BUL17/2/11	6.94	Quartz	15/15	1.64±0.16	8.31±0.83	1.36±0.14	0.10±0.01	2.50±0.18	6.4	80.40±1.90	32.18±2.39	31.50±1.65
BUL17/2/9	7.40	Quartz	15/15	1.75±0.18	8.07±0.80	1.39±0.14	0.09±0.01	2.53±0.18	0.0	85.00±1.30	33.56±2.40	32.46±1.73
BUL17/2/7	8.00	Quartz	15/15	1.88±0.19	9.02±0.90	1.45±0.14	0.09±0.01	2.70±0.19	0.0	86.70±1.40	32.11±2.34	33.08±1.84
BUL17/2/6	8.50	Quartz	15/15	1.93±0.19	9.41±0.94	1.61±0.16	0.08±0.01	2.89±0.20	0.0	94.35±2.07	32.67±2.40	34.17±2.14

BUL17/2/5	9.00	Quartz	15/15	2.01±0.20	9.89±0.99	1.62±0.16	0.08±0.01	2.96±0.21	7.3	111.79±3.14	37.80±2.86	37.96±2.93
BUL17/2/3	10.0	Quartz	15/13	1.97±0.20	9.48±0.95	1.49±0.15	0.07±0.01	2.79±0.20	0.0	143.68±5.86	51.54±4.22	49.75±3.51
BUL17/2/2	10.5	Quartz	17/17	1.86±0.19	10.12±1.01	1.72±0.17	0.07±0.01	3.22±0.23	6.7	153.12±3.69	50.83±3.78	52.31±3.73
BUL17/2/1	13.7	Feldspar	15/15	1.78±0.18	9.38±0.94	1.43±0.14	0.05±0.01	2.65±0.19	2.5	271.57±4.48	95.53±6.00	95.72±6.52

3.4. Provenance

Most studies characterising the provenance of loess along the Danube have relied on bulk geochemical analyses (Buggle et al., 2008; Schatz et al., 2015; Újvári et al., 2014b, 2008) that may provide incomplete or limited information about loess provenance (Stevens et al., 2010). A significant body of work carried out using single-grain approaches on the Chinese Loess Plateau has transformed understanding of the provenance of loess deposits (Bird et al., 2015; Fenn et al., 2018; Licht et al., 2016; Nie et al., 2015). To date, only a handful of loess profiles in Europe investigated provenance with single-grain provenance methods (Pańczyk et al., 2020; Újvári et al., 2012; Újvári and Klötzli, 2015). While these studies have focused on understanding and characterising sources of the sediment, no study has used the provenance signal to investigate the evolution of LPS and to support the palaeoenvironmental reconstruction of a site.

Zircon U-Pb data for both Slivata profiles presented by Fenn (2019) was replotted at the site resolution to provide a better understanding of the palaeoenvironmental history of the site. To statistically analyse provenance results two approaches were used: Kernel Density Estimation (KDEs), that provides visual assessment of U-Pb age distributions (Andersen et al., 2018; Vermeesch, 2012); and Multi-Dimensional Scaling (MDS; Vermeesch, 2013), that investigates the similarity between large numbers of datasets, allowing a comparison. KDEs for each sample were plotted in the detzrcr R package (Andersen et al., 2018) using the same bandwidth of 30 Ma. MDS is based on Kolmogorov-Smirnov (KS) statistics, which outputs a two-dimensional diagram where similarity/dissimilarity is represented as a relatively short/large distance between samples. In this paper the MDS was computed using the “non-metric” algorithm in IsoplotR and stress value (goodness of fit) determined by plotting a ‘Shepard plot’ (Vermeesch, 2018).

4. Results

4.1. Particle size

Overall grain size distribution shows a typical unimodal distribution with a peak in the silt fraction and a tail in finer grain sizes (Supplementary Figure S1). Throughout the Slivata 1 profile coarse silt (31-62 μm) is the most abundant grain size fraction (Figure 4), closely followed by very fine sand in Units VI and VII and fine silt (8-16 μm) in Unit III. Particle size generally fines upward, and is driven by both the decrease in the proportion of sands (from ~30% to less than 20%), and increase in the content of clay, which changes from 5 to 15%. The highest U-ratio values (above 3) occur between 5 – 5.75 m, peaking at 5.7 m (3.75). While the U-ratio shows a general upwards decreasing trend and stabilisation in the top 2.5 m around 2, the change below 2.5 occurs in an oscillatory step manner.

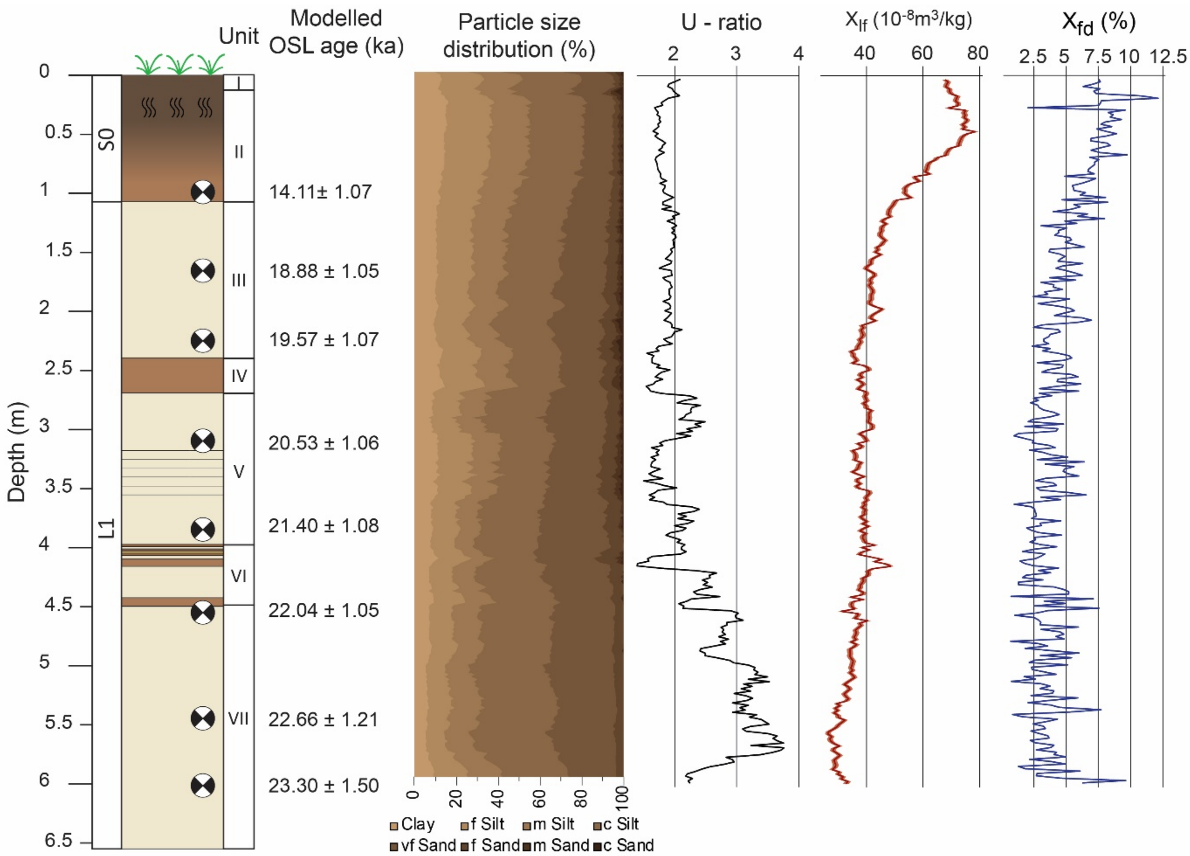

Figure 4. Stratigraphic log of Slivata 1 sedimentary units (Figure 3), modelled OSL ages, particle-size distribution of all sedimentary fractions, the U-ratio, and magnetic susceptibility (presented as low-frequency (χ_{lf}) and frequency dependant (χfd %) values). Please note we use <5 μm for clay fraction.

The initial field assessment indicated that the upper parts of the Slivata 2 profile contains thick "primary" loess deposits (Figure 2C), and that stratigraphic horizons between Slivata 1 and 2 overlapped, therefore samples at Slivata 2 were collected only between Units IV and X (Figure 3). However, cleaning, detailed logging and description, and laboratory analysis revealed that these profiles are much more spatially complex and do not overlap in the initially anticipated manner. Therefore, the sedimentological data for Slivata 2 covers Units VI and X and these units are the focus of the Slivata 2 analysis and discussion.

At Slivata 2 particle size is also dominated by coarse silt (30-40% of the distribution) and is closely followed by medium silt and very fine sand (Figure 5). Clay content stays relatively stable throughout the profile, oscillating around 10%. A broadly coarsening trend occurs with a switch at ~8.15 m when very fine sand becomes the second most dominant particle size fraction (from 15% to as much as 27%). Below the 8.15 m depth medium and fine silt contribute

20-25% each to the distribution. The overall particle size distribution at Slivata 2 (Figure 5) shows much more variability than Slivata 1 (Figure 4), especially between 6.7 m and 7.8 m where erratic shifts in the proportions of clay and sand occur. This is also reflected in the U-ratio changes for that part of the profile, where the shifts are abrupt. For example, in Unit VII shifts in values are as high as 1.25 between neighbouring samples. The U-ratio shows a general increase in values (2 to 2.7) from the bottom of the section upwards.

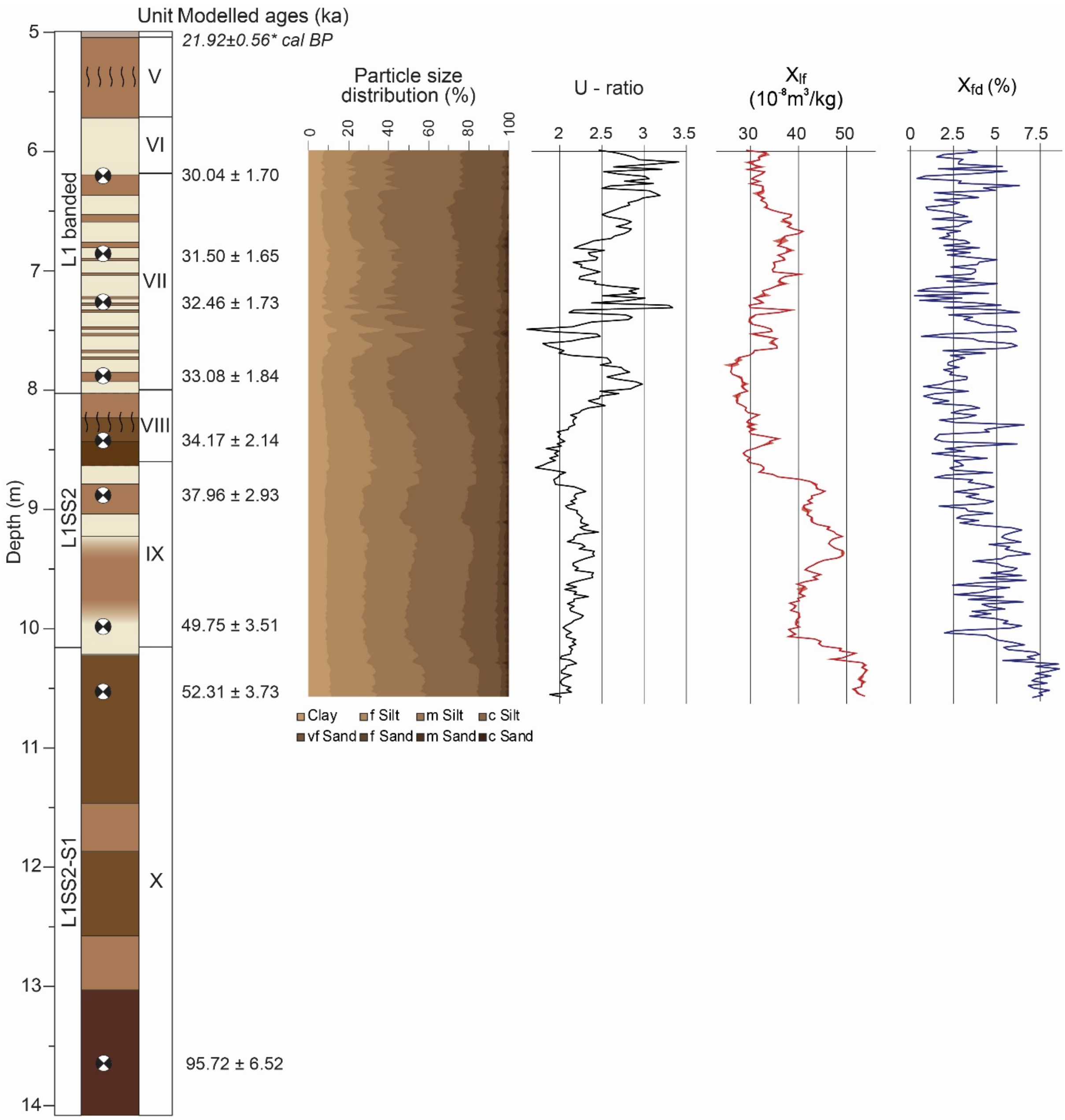

Figure 5. Stratigraphic log of Slivata 2, sedimentary units (Figure 3), modelled OSL ages, particle-size distribution of all sedimentary fractions, the U-ratio, and magnetic susceptibility (presented as low-frequency (χ_{lf}) and frequency dependant (χfd %) values). *- denotes age

based on the identification of Cape Riva/Y-2 tephra sample. Please note we use <5 μm for clay fraction.

4.2. Magnetic susceptibility

At Slivata 1 magnetic susceptibility (χ_{lf}) values generally decrease with depth (Figure 4), with a classic pattern of low values in loess (min 27 x 10^{-8} m^3 kg^{-1} below 5 m) and enhanced ones in palaeosols (78 x 10^{-8} m^3 kg^{-1}). The χ_{lf} values gently increase from 30 to 40 (x10^{-8} m^3 kg^{-1}) in Unit VII, but remain relatively constant until 1.5 m, after which they gradually rise. Additionally, two small peaks of relatively enhanced χ_{lf}, at ~2 m and ~4 m, occur. The frequency-dependent (χfd %) record, while variable in loess Units VII-III, is mostly oscillating between 2-5%. Around 1.5 m the χfd values increase and centre around 7.5% in the soil (Unit II). At 0.3 m χfd values drop drastically from 7.5% to 2%.

At Slivata 2 magnetic susceptibility values broadly increases with depth (Figure 5), however the shifts are not as straightforward as an increase in pedogenic horizons and low values in loess units. The χ_{lf} values rise slightly in the middle of Unit VII, but decrease and become very irregular after 7 m with some large peaks towards the bottom of the unit (e.g. 7 m and 7.3 m). Magnetic enhancement occurs at 8.5 m where the values begin to rise (top of Unit IX) and following a short drop in the more “loess-like” sediment (bottom of Unit IX), rise to their highest value (55 x 10^{-8} m^3 kg^{-1}) in Slivata 2. The χfd is also highly variable across the whole profile. It decreases upwards in two step-like shifts from Unit X to Unit IX (10.15 - 9 m). The third shift, through the top of Unit VIII, has a more gradual trend. In both profiles not all changes in the χ_{lf} correspond to shifts in χfd (e.g. Unit VII in Slivata 2), suggesting an additional influence on the inferred pedogenic signal.

4.3. Tephra interpretation

Results of geochemical analysis of individual glass shards (n=46) from the tephra sample found in Slivata 2 are presented in Table 1, with bi-plots of selected major elements presented in Figure 6. The geochemical composition of analysed shards from Slivata 2 shows a homogenous rhyolitic affinity (high SiO_2 content 72.65 ± 0.55 wt%). Further the composition is characterised by relatively high CaO and MgO contents, of 1.73 ± 0.09 wt% and 0.43 ± 0.03 wt% respectively. The consistent geochemical clustering (Figure 6), supported by the chronostratigraphic position at Slivata 2, indicates that the tephra layer can be correlated with the Cape Riva (Y-2) tephra, erupted from the Santorini volcanic centre (Druitt, 1985; Vespa et al., 2006). The age of the Cape Riva eruption was modelled by Lee et al. (2013) based on terrestrial radiocarbon datasets from Lesvos, Greece (Margari et al., 2009), Lake Iznik, Turkey (Roeser et al., 2012), and Tenaghi Philippon (Müller et al., 2011). The Lee et al. (2013) Oxcal model was re-run using the IntCal20 calibration curve (Reimer et al., 2020) and luminescence ages originally provided by the Roeser et al. (2012). This provided a revised modelled age of 21.92±0.56 cal ka BP (Supplementary Materials Figure S2 and Table S3).

While ash correlated to the Cape Riva/Y-2 eruption has been reported widely in marine deposits (Kwiecien et al., 2008; Satow et al., 2015; Wulf et al., 2002) in the terrestrial realm it has only been reported as far as mainland NE Greece (Müller et al., 2011; Seymour et al., 2004). Therefore, the recovery of tephra from the Cape Riva/Y-2 eruption in Northern Bulgarian loess extends the known dispersal area for the fine ash from this eruption further into the continent. Based on these findings, the Cape Riva/Y-2 provides a potential chronostratigraphic marker for loess deposits in Central and Eastern Europe during the Last Glacial Maximum (LGM).

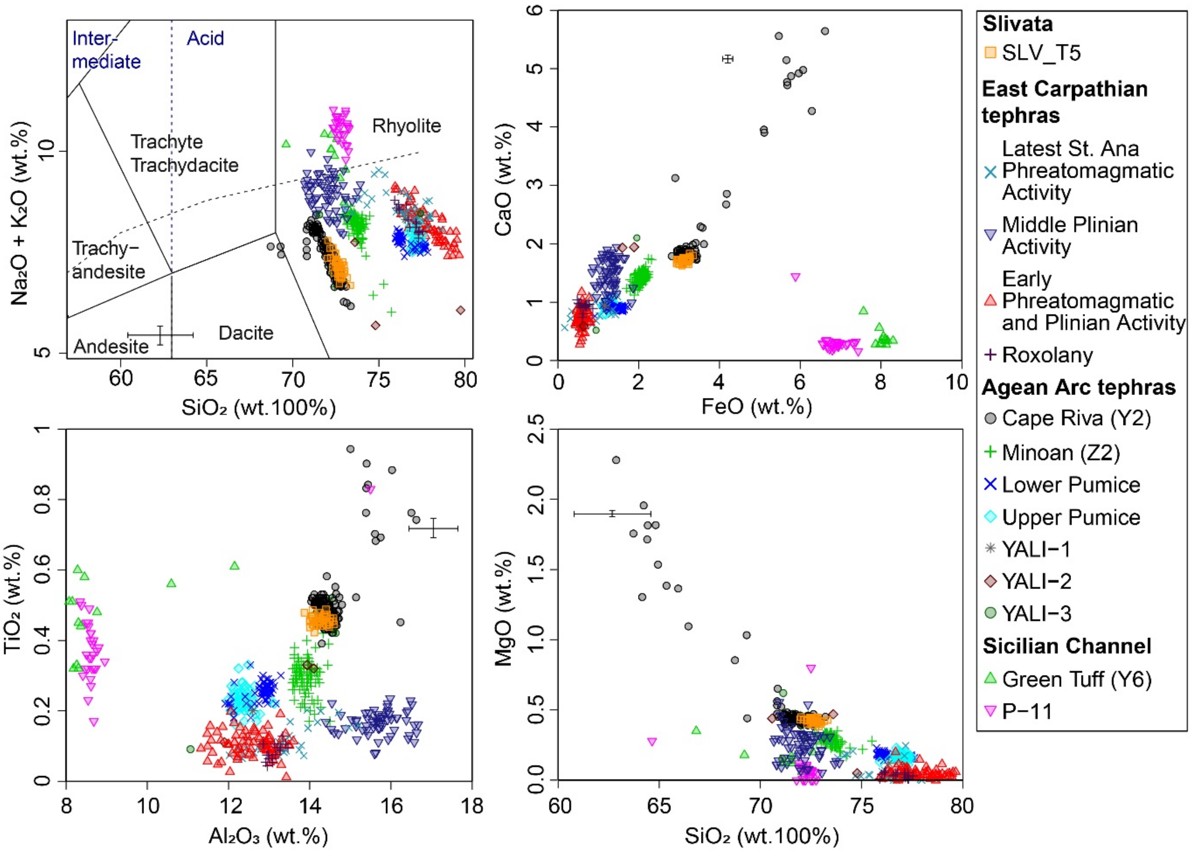

Figure 6. Geochemical bi-plots of the major and minor element oxide data from Slivata 2 (sample code SLV_T5), plotted with known rhyolitic eruptions from volcanic sources in East Carpathian and Mediterranean Region. Reference tephras for East Carpathian Volcanic Range (Early Phreatomagmatic and Plinian Activity (EPPA): Karátson et al. 2016; Middle Plinian Activity (MPA): Karátson et al. 2016; Latest St. Ana Phreatomagmatic Activity (LSPA): Karátson et al. 2016; Roxolany: Wulf et al. 2016), Aegean Arc (Cape Riva (Y-2): Kwiecien et al., 2008; Margari et al., 2007; Tomlinson et al., 2015; Wulf et al., 2002; Minoan (Z2): Eastwood et al., 1999; Kwiecien et al., 2008; Tomlinson et al., 2015; Nisyros Upper and Lower Pumice:

Karkanas et al., 2015; Tomlinson et al., 2015; YALI: Federman and Carey, 1980; Hardiman, 2008; Vinci, 1985; and Sicilian Channel Sicilian Channel (Green Tuff (Y-6): Vogel et al., 2010; P-11: Karkanas et al., 2015; Lézine et al., 2010; Paterne et al., 2008). Error bars show 2 standard deviations of repeat analysis of the StHs6/80-G MPI-DING standard glass.

4.4. Chronology

4.4.1. Luminescence dating assessment

The interpretation of the complex stratigraphic and sedimentary records preserved within the LPS at Slivata requires a careful consideration of chronological reliability. Samples were collected predominantly from aeolian deposits and the field investigation (Figure 3) revealed no signs of sediment displacement as a result of e.g. solifluction or cryoturbation. Further, areas affected by bioturbation were avoided. Therefore, it is likely that the dated aeolian material was bleached during transport and results reliably constrain the age of burial.

Detailed results of the luminescence tests are provided in supplementary materials. In summary, for quartz the selected 240°C preheat performed well in the dose recovery tests with all aliquots passing within uncertainties and an average dose recovery of 1.0±0.05 (Supplementary Materials Figure S3 and Table S4). Quartz OSL signals (Supplementary Material Figures S4) decay rapidly to near background levels within a few seconds of stimulation, indicating dominance of the fast component in the initial part of the signal (Durcan and Duller, 2011). Based on the combined preheat plateau and dose recovery test (0.98±0.05), the post-IR $IRSL_{225}$ ($pIRIR_{225}$) protocol was selected for sample BUL17/2/1. The signal from the feldspar pIRIR protocol does not fade above the accepted measurement detection levels (Supplementary Figure S4). These intrinsic luminescence signal characteristics indicate the suitability for dating of the selected luminescence signal.

4.4.2. Luminescence ages and MARs

Whilst Bayesian modelling of luminescence ages results in the reduction of age uncertainties, even after modelling, uncertainties of ~6% are associated with the modelled ages in this study. This, along with the resolution of ages, gives rise to discrepancies between the calculated minimum and mean MARs. To reflect chronological uncertainties, both minimum and mean values are presented (Figure 7 and Supplementary Figure S8), which allows for investigation and comparison of trends between the range of values. In the case of Slivata, the direction of change remains broadly similar for minimum and mean values, thus giving confidence in the relative dust flux increases and decreases at the presented timescales. In all cases minimum and mean values are presented and the directional trends observed, rather than individual values, should be the focus.

The results of luminescence dating are presented in Table 2, and Figures 4 and 5. OSL data from the Slivata 1 profile provide age constraints ranging from 23.30±1.50 ka at 6 m depth to 14.11±1.07 ka just at the transition to the Holocene topsoil (1 m depth) (Figure 4). The mass accumulation rates based on the OSL data (Figure 7) show significant variability regardless of whether minimum or mean accumulation rates are investigated (Supplementary Materials Figure S8). Two peaks in MARs occur at Slivata 1 and both are associated with the Last Glacial Maximum; the first one between 22.66±1.21 ka and 22.04±1.05 ka (mean= 2413 g m^{-2} a^{-1}, minimum= 521 g m^{-2} a^{-1}), and the second one between 19.57±1.07 ka and 18.88±1.05 ka (mean= 1524 g m^{-2} a^{-1}, min= 374 g m^{-2} a^{-1}).

At Slivata 2 (Figure 5) the upper and lower chronological control points date to 21.92±0.56 cal BP (Unit IV) the Cape Riva/Y-2 eruption tephra horizon; and the luminescence age of 95.72±6.52 ka for the palaeosol (Unit X) at the bottom of the analysed profile. The top of Unit X to the bottom of Unit VI cover the period between 30.04±1.70 ka and 52.31±3.73 ka. A peak in mass accumulation rates occurs between 32.46±1.73 ka and 33.08±1.84 ka (Unit VII), where rates reach a mean value of 1339 g m^{-2} a^{-1} (Figure 7) (min= 220 g m^{-2} a^{-1}; Figure S.6). This peak is part of a temporary enhanced phase of sediment accumulation associated with the loess punctuated by the palaeosol-like bands (Unit VII) that occurred between 33.08±1.84 ka and 30.04±1.70 ka.

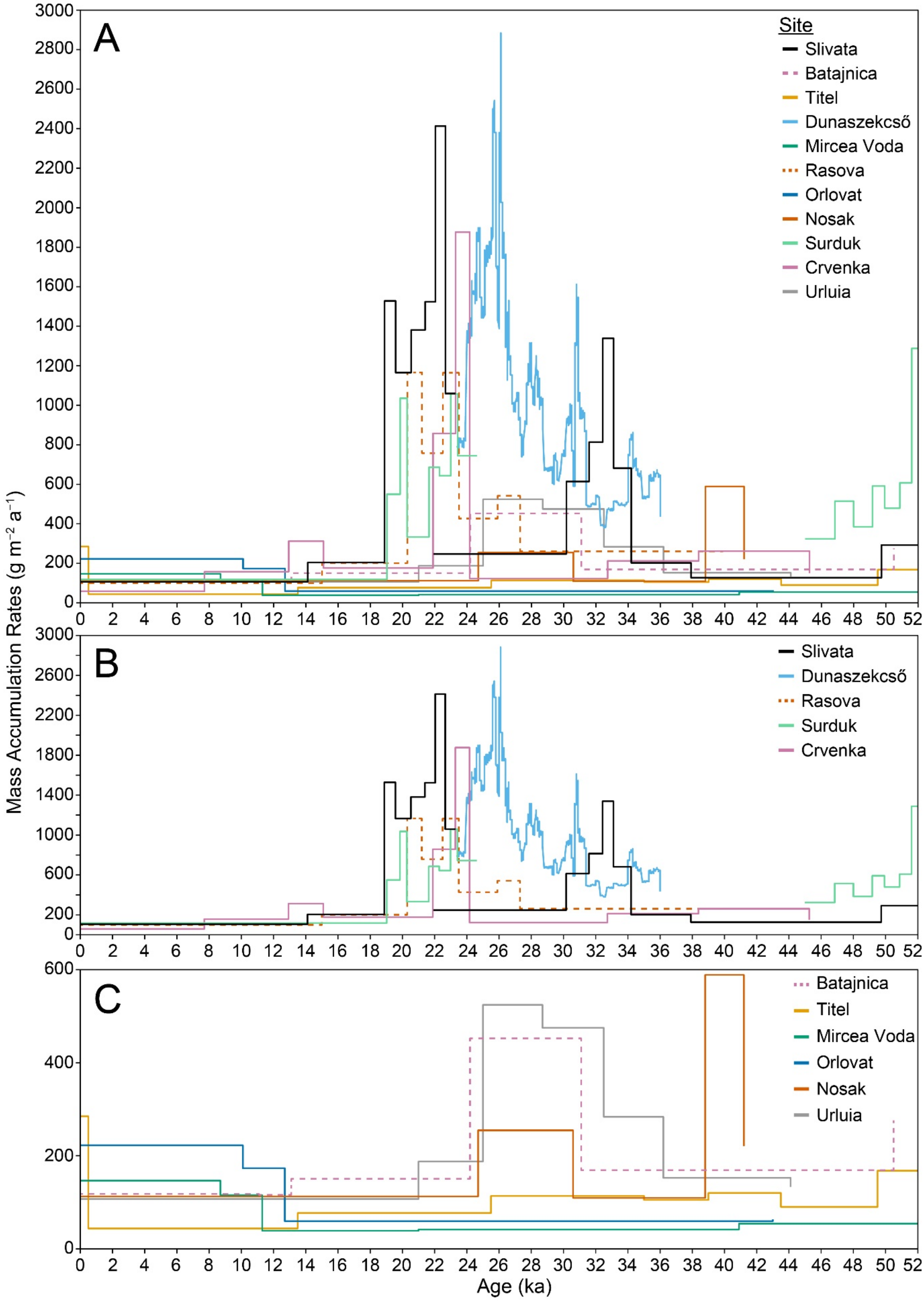

Figure 7. Mass accumulation rates (MARs) as a function of age for the loess–palaeosol profiles. A) Results for Slivata plotted against remodelled results from Batajnica (Avram et al.,

2020), Crvenka (Stevens et al., 2011), Dunaszekcs (Újvári et al., 2017), Mircea Voda (Timar-Gabor et al., 2011), Nosak (Perić et al., 2020), Orlovat (Marković et al., 2014b), Rasova (Zeeden et al., 2018c), Surduk 2 (Fenn et al., 2020b), Titel (Perić et al., 2019), Urluia (Obreht et al., 2016). Panels B) and C) show the same data as A) but focus on sites with MARs above 600 g m^{-2} a^{-1} and below 600 g m^{-2} a^{-1} respectively. The locations of all sites are shown in Figure 1.

4.5. Provenance

Figure 8A shows that the majority of the zircon U-Pb grains at the Slivata 1 profile are of 200-800 Ma age. Additional populations, albeit much smaller, of Precambrian ages can be seen. Most samples at both profiles also contain very young (<100 Ma) zircon grains. Broadly three populations are observed at ~300 Ma, ~450 Ma, and ~600 Ma, however in some samples only two of the three populations are distinct. At Slivata 1 ~450 Ma grains are abundant, apart from samples BUL17/1/3 and BUL17/1/5 (sediment deposited at 19.57±1.07 and 20.53±1.06 ka respectively) where this Ordovician population is subordinate. Further, the Carboniferous population (~300 Ma) does not seem to contribute greatly to the age distribution in sample BUL17/1/11 (loess deposited at 22.66±1.21 ka).

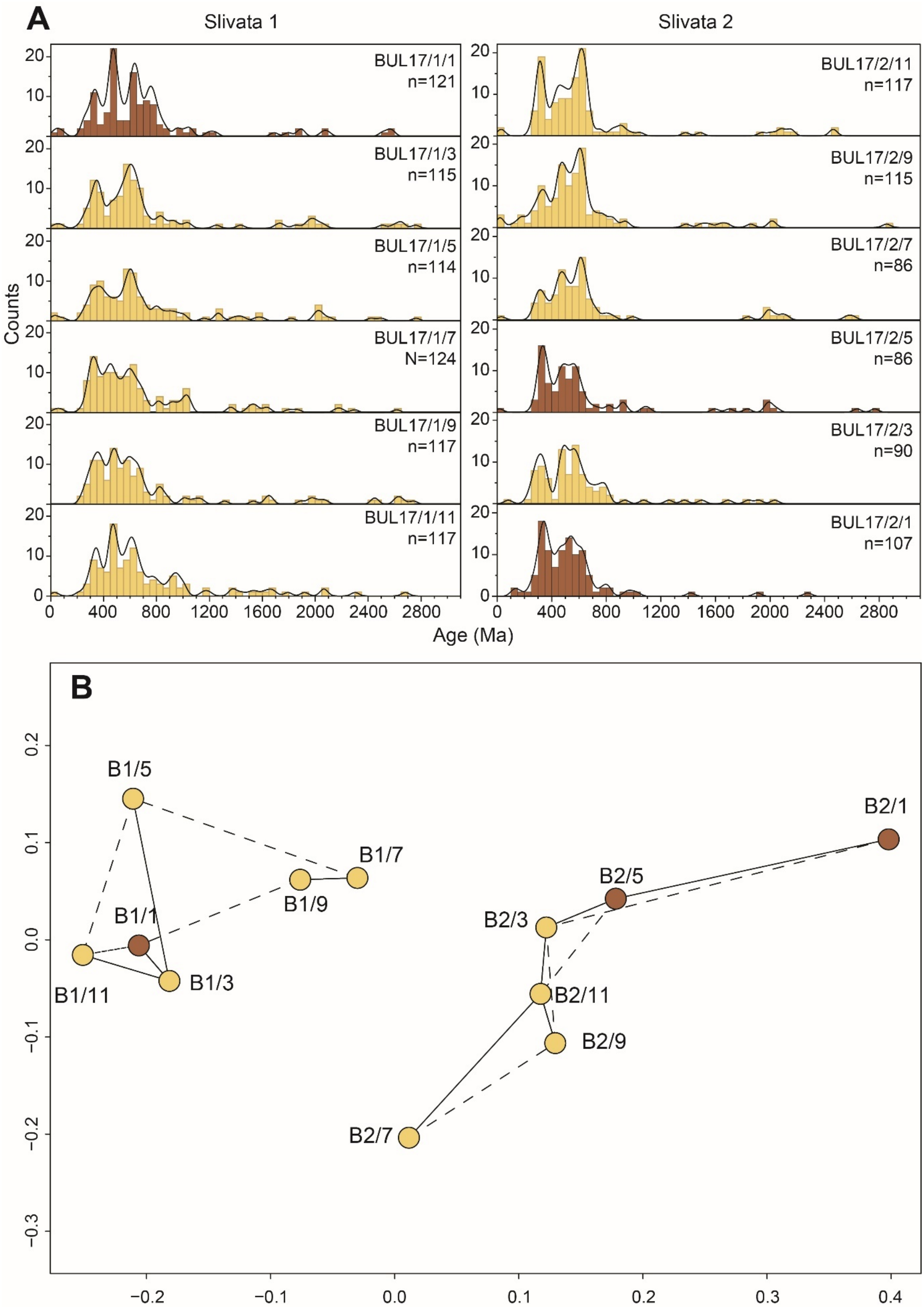

Figure 8. Zircon U-Pb results for both Slivata loess- palaeosol profiles. A) Kernel Density Estimator (KDE) diagram. Samples are presented in stratigraphic order and colours denote

loess vs palaeosol samples. Based on a 30 Ma bandwidth. B) Multi-dimensional scaling (MDS) map for data A, showing individual samples from both Slivata profiles. Full lines connect the two most similar samples, whereas dotted lines show the second closest data matches. For clarity, sample codes for samples are shortened (e.g. BUL17/1/1 is B1/1). Stress value = 6.25%.

KDEs for Slivata 2 show that most grains are of Mesozoic-Palaeozoic age. There is also an indication of three distinct peaks in some distributions, although in BUL17/2/3 and BUL17/2/5 (deposited at 49.75±3.51 and 37.96±2.93 ka respectively) they are not as apparent. This could be an artefact of the smaller number of grains yielding concordant ages. The abundance of the ~600 Ma population shifts down the section, as it changes from the dominant to subordinate (from sample BUL17/2/5 down). Additionally, in the bottom three sample contributions from 450 Ma grains are almost equal to the 600 Ma, creating more of a plateau than a peak. In all Slivata 2 samples the ~300 Ma population observed is one of the more dominant, apart from samples BUL17/2/7 and BUL17/2/9 (sediment deposition at 33.08±1.84 and 32.46±1.73 ka). In the case of the former this is possibly due to a smaller number of grains analysed, but this is not the case for the latter. The proportion of grains forming the ~450 Ma population is variable between samples. Finally, very young grains (<100 Ma) are in all but the bottom two samples.

5. Discussion

5.1. Sediment production and transport

The U-Pb zircon dating results presented are the first attempt at utilising single-grain provenance data to support an interpretation of a complex Quaternary stratigraphic and sedimentary record. In the first instance Figure 8A suggests that all samples have very similar distributions, all containing grains in the dominant triple populations of 300 Ma, 450 Ma, and 600 Ma. The MDS map (Figure 8B), that is a graphical way of plotting similarities between datasets, does not show any overlap between Slivata 1 and Slivata 2 samples. Further the nearest neighbour lines, which connect most similar (solid line) and second most similar data points (dashed line), also do not cross over between Slivata 1 and Slivata 2. Combining samples to create an average Slivata 1 and average Slivata 2 sample and plotting them as Cumulative Age Distributions (CADs) (Supplementary Material Figure S9) shows that Slivata 2 comprises more grains <650 Ma, whilst Slivata 1 has more Neoproterozoic and Mesoproterozoic grains, though both distributions have a similar shape suggesting predominantly the same source rocks. The initial divergence between Slivata1 and Slivata 2 populations occurs at ~300 Ma, with two additional and larger inflections at 500 Ma and 600-

650 Ma by which point there is 15% difference between two distributions. Based on zircon U-Pb ages and Hf isotopes Fenn (2019) showed that the provenance signal in Danubian loess sequences is spatially homogenous. They also suggested small variations observed in the averaged site samples likely come from episodic contributions from the local bedrock. Neoproterozoic and Cambrian aged igneous rock outcrops are not very abundant in relative proximity to the Lower Danube. Though, the western part of the Balkan Mountains, in the foothills of which the Slivata loess profiles are located, comprise Cambrian age, island-arc associated igneous rocks (Haydoutov, 1989; Haydoutov and Yanev, 1997). Gabbro rocks in the Tcherni Vrah massif were dated to 563±5 Ma (Savov et al., 2001) and granitoid rocks in its vicinity provided ages of 527±18 Ma (Plissart et al., 2012). These ages overlap with the ages that cause offset between Slivata 2 and Slivata 1 zircon samples, therefore suggesting that Balkan Mountains were providing some contributions to the Slivata 2.

As Slivata 1 and 2 loess profiles cover two different depositional time periods, MIS 2 and MIS 3 respectively, the dissimilarity in source between two sites suggest that that at some point in the transition between MIS 2 and MIS 3 the sediment generation and delivery from the Balkan Mountains dropped. Alternatively, it is possible that during MIS 2 the sediment supply from the surrounding mountain belts increased and the dominant zircon ages, the "average" Danube loess signal Fenn (2019), suppressed the signatures supplied by the Balkan Mountains.

5.2. Palaeoenvironmental reconstruction

5.2.1. MIS 5 and MIS 4

The thick, welded pedocomplex underneath Slivata 2 (Figures 2 and 3) is thought to correspond to palaeosols S1-S4 at Orsoja (Avramov et al., 2006), on top of which rests a well-developed palaeosol (Unit X in Figure 5). Based on luminescence ages sediment deposition for this unit commenced around 95.72±6.52 ka and concluded shortly after 52.31±3.73 ka (Figure 5). Whilst luminescence dating does not provide an age for palaeosol development, this suggests that at the onset of the glacial period (equivalent to the transition from MIS 5c to MIS 4) pedogenic processes exceeded the aeolian contributions which resulted in a prominent palaeosol at the base of the Slivata profile. The strong pedogenic signal is supported by the position of the L1SS2-S1 (palaeosol developed at the bottom of the last glacial loess and last interglacial palaeosol (Units IX and X)) samples on the $\Delta\chi$ and χlf plot (Figure 9A), mostly overlapping with the "true loess line", indicating climatically controlled weathering enhancement. This is in contrast with other sites along the Romanian Plain, such as Harletz (Antoine et al., 2019; Avramov et al., 2006; Lomax et al., 2018), Viatovo (Balescu et al., 2020; Jordanova et al., 2007), and Kaolinovo (Balescu et al., 2020) where S1 palaeosol is only about half as thick as Slivata's 2 (Figures 3 and 5). The S1 palaeosols thicken in the Dobrogea and proximity to the Black Sea (Fitzsimmons, 2017; Timar-Gabor et al., 2011; Vasiliniuc et al., 2011), further supporting localised controls on the palaeosol development.

Across both Middle and Lower Danube sites, e.g. Batajnica (Avram et al., 2020), Costineşti (Constantin et al., 2014), Orlovat (Marković et al., 2014b), or Semlac (Zeeden et al., 2016) loess deposition during MIS 4 period is typically recorded, suggesting that a record of the early glacial is missing or has been overprinted by pedogenesis at Slivata. Therefore Slivata 2 might present a case similar to Crvenka (Marković et al., 2018b; Stevens et al., 2011) where the authors argued for an erosion of the early glacial loess. However, thick palaeosol for this period also occurs at Nosak (Perić et al., 2020), a site on the other side of the Carpathian Mountains, which could suggest that both the Nosak and Slivata experienced microclimate conditions during the early stages of the last glacial period which resulted in enhanced pedogenesis during this period.

5.2.2. MIS 3

During MIS 3, loess deposition at Slivata 2 began around 49.75±3.51 ka and continued until sometime after 30.04±1.70 ka (Figure 5), however this period is punctuated by a series of fairly well-developed palaeosols (e.g. Units IX and VIII) and thin palaeosol-like horizons (Unit VII). The pedogenic horizons in Units IX and VIII developed 49-33 ka, and broadly correspond to a shift in χfd (which decreases is a step manner), relatively low U-ratio values (Figure 10), and mean mass accumulation rates below 300 g m^{-2} a^{-1} (Figure 7; min >100 g m^{-2} a^{-1}), all of which indicate a generally gradual climate deterioration and aridification punctuated by temporarily stable environments. The palaeosol horizons in Unit IX, whilst variable, generally show an increase in χfd, which translates to a cluster around the “true loess” trendline on the $\Delta\chi$ and χlf diagram (Figure 9A), suggesting magnetic enhancement is controlled by the climatically driven weathering of loess (Forster et al., 1994). The well-developed palaeosol in Unit VIII corresponds to a lowering in χfd and plots mostly below the trendline on Figure 9 and points to hydromorphy and a reduction of magnetic particles. As no periglacial features are observed this suggests either periodic waterlogging and/or wetter conditions between 34-33 ka. These periods broadly coincide with periodic Black Sea surface water temperature increases (Figure 10) but also the onset of ice rafting (Wegwerth et al., 2015), indicating longer winters and likely strong seasonal temperature gradients, which could drive seasonal water logging. The $\delta^{18}O$ data from Tăuşoare (Figure 10) and Ascunsă Caves (Staubwasser et al., 2018) also shows periodic temperature shifts during MIS 3 which are thought to represent regional climatic shifts. Broadly speaking therefore, MIS 3 appears to be stable enough to promote enhanced pedogenesis but the conditions deteriorated gradually until the MIS 2 transition. Palaeosol development is also seen at Nosak (Marković et al., 2014a; Perić et al., 2020), on the other side of Iron Gorge, which could suggest that for both Slivata and Nosak the Carpathian Mountains had an amplifying effect on seasonality and resulted in more localised paedogenesis.

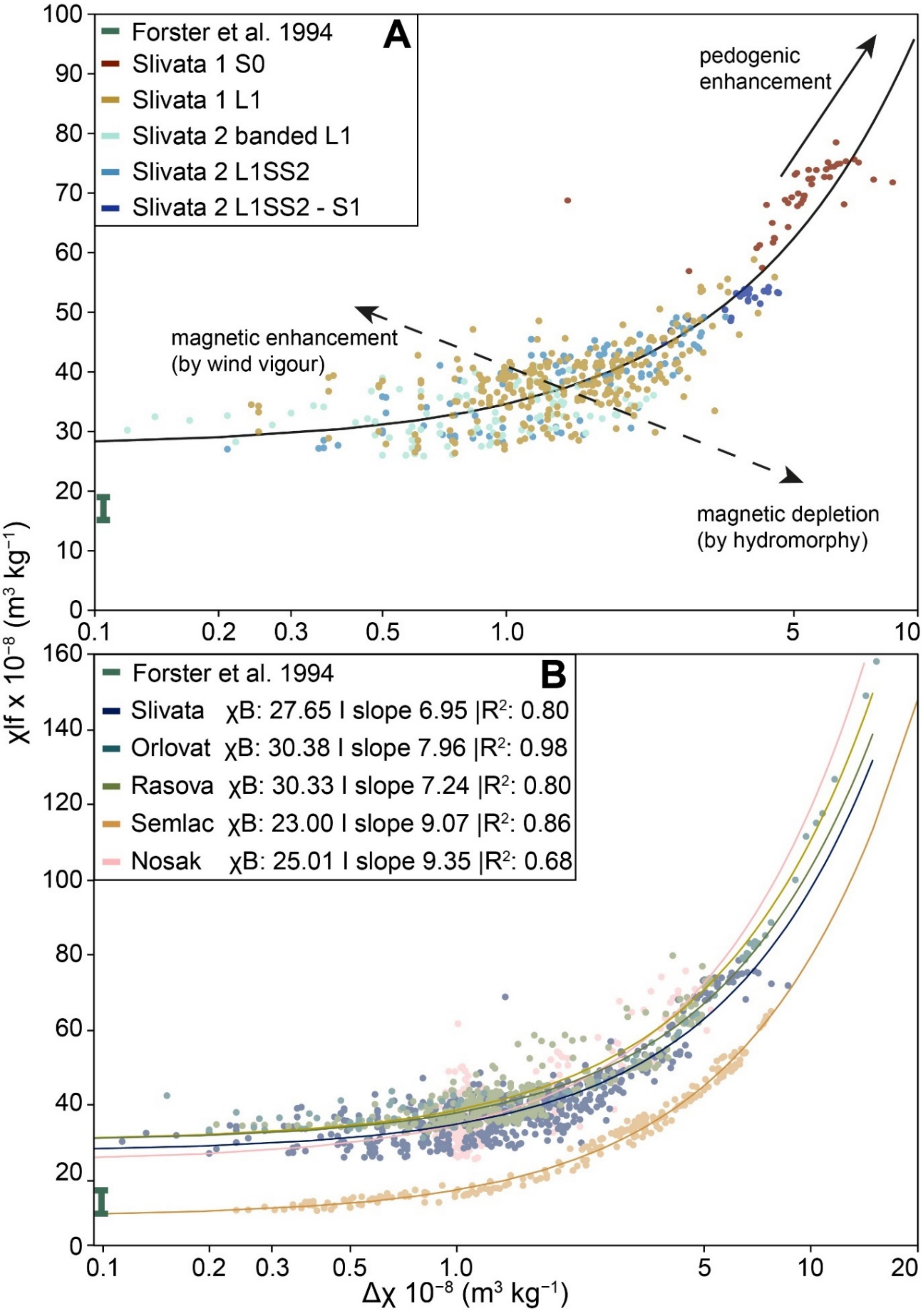

Figure 9. Magnetic enhancement plots for (Δχ (absolute) vs χlf) compared with Forster et al. (1994) background susceptibility of "raw dust" Chinese and Central Asian loess. A) Slivata 1

and 2 samples divided into the main chronostratigraphic units following (Marković et al., 2008); S0 – Holocene soil, L1 – last glacial loess, S1 – last interglacial palaeosol. The black line marks the best fit line ("true loess line") to the whole Slivata dataset. B) Comparison of Slivata magnetic enhancement with Orlovat (Marković et al., 2014b), Rasova (Zeeden et al., 2018c), Nosak (Marković et al., 2014a), and Semlac (Zeeden et al., 2016) and their individual background susceptibilities.

The most striking feature of the Slivata 2 loess-palaeosol sequence is Unit VII (Figures 2, 3, and 5). This loess-palaeosol complex comprises 13 thin reddish-brown palaeosol-like horizons interbedded with typical loess, that were deposited/developed 33-30 ka, occurring on average every ~20-506 years. The χfd is highly variable, though a slight decreasing trend is noted (Figure 11), despite the presence of the palaeosol-like features. The thin palaeosol-like features also show an increase in the magnetic signal. At the same time, the U-ratio and sand content (~30%) increase (Figure 10), especially in the loess bands sandwiched between palaeosol-like features. The mean mass accumulation rates increase to 1339 g m^{-2} a^{-1} (min 220 g m^{-2} a^{-1}); the highest values for the Slivata 2 profile (Figure 7), suggesting a very dynamic aeolian environment, strong winds, increasing sediment supply, proximal source, and a distinctive end to MIS 3.

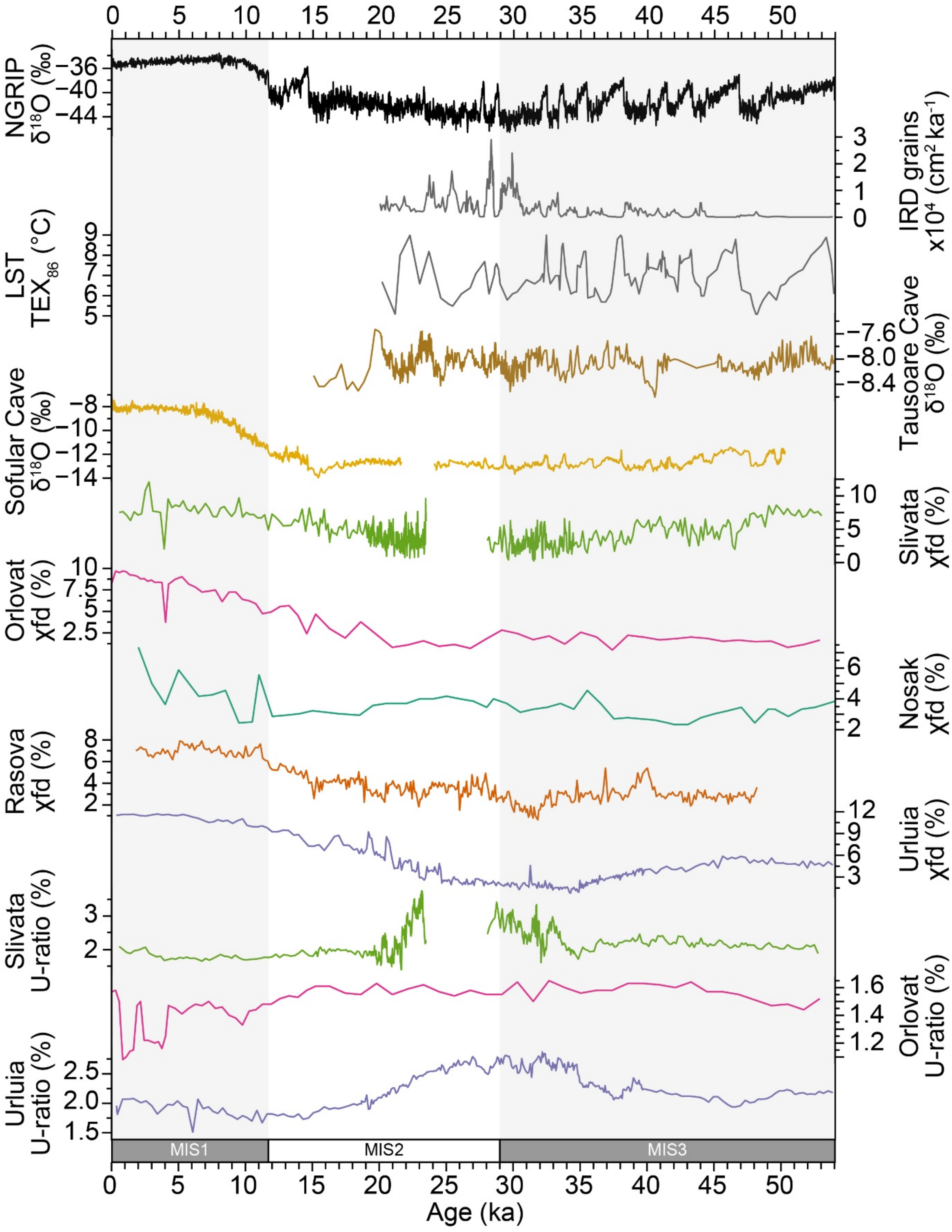

Figure 10. A comparison between Greenland's NGRIP δ^{18}O (Rasmussen et al., 2006); Black Sea coastal ice-rafted detritus (IRD) and lake surface temperature (TEX$_{86}$) (Wegwerth et al., 2015); Tăuşoare Cave δ^{18}O (Staubwasser et al., 2018); Sofular Cave δ^{18}O (Fleitmann et al., 2009); Orlovat χfd (Marković et al., 2014b), and U-ratio and >63 μm (Obreht et al., 2015);

Nosak χfd (Marković et al., 2014a; Perić et al., 2020), Rasova χfd (Zeeden et al., 2018c), Urluia χfd and U-ratio (Obreht et al., 2017).

Data from this unit plots either above or below the “true loess” trendline (Figure 9A), with very few points plotting on the line. The samples to the left of the line (elevated χlf and reduced Δχ) can be better explained by the ‘wind vigour model (Maher, 2011; Zeeden et al., 2018c), where the enhancement in χlf is likely driven by the incorporation of the coarser ferromagnetic grains, therefore supporting short phases of increased winds, and likely gusty and dry climatic conditions. The samples to the left of the line (reduced χlf and elevated Δχ) are more aligned with the ‘hydromorphy models’ (Baumgart et al., 2013; Zeeden et al., 2018c) where the waterlogging conditions cause dissolution of magnetic particles. The primary drivers of hydromorphic depletion in loess are periglacial conditions (Baumgart et al., 2013; Gocke et al., 2014). Whilst there is no indication that Slivata was in a continuous permafrost zone (Lehmkuhl et al., 2021), discontinuous permafrost zone was located in the relative proximity to the site (Ruszkiczay-Rüdiger and Kern, 2016; Vandenberghe et al., 2014a) therefore Slivata could have been affected by at least deep seasonal frost, but possibly by sporadic and isolated permafrost which caused temporary waterlogging and some reduction in χ. Crucially the enhancement observed for the palaeosol-like banded units is unlikely to be climatically driven and not does not indicate pedogenesis at that time.

The Black Sea lake temperature (Figure 10) and ice-rafted debris records indicate that the region was experiencing increasing seasonality and progressively longer and colder winters, likely in relation to the growth of the Fennoscandian Ice Sheet (Shumilovskikh et al., 2014; Wegwerth et al., 2015) and smaller glaciers in the Carpathian and Balkan Mountains. Tăuşoare Cave (Figure 10) also shows a highly variable $\delta^{18}O$, interpreted as fluctuations in regional hydrologic conditions (Staubwasser et al., 2018). These, combined with decreasing boreal vegetation cover (Connor et al., 2013), strong seasonality, and periodical ice melting (Rostek and Bard, 2013; Wegwerth et al., 2016), could lead to periods of increased and intermittent soil erosion especially on the higher ground. Whilst at present Slivata rests at the top of the hill (transect A’-A), transect B’-B shows a slope towards the Danube (Figure 2). Further the modern topography cannot be taken as representative of the paleotopography 30 ka ago especially given that Unit VII is covered by 6 meters of sediment. Consequently the palaeosol-like horizons could represent the disturbance of the primary loess deposition by the sheet wash and deposition of soil material eroded from upslope loess sequences (Figure 2A and 2E) during periods of seasonal melting. The grain size, magnetic susceptibility, as well as the time factor suggest that *in situ* pedogenesis for these units is unlikely. This interpretation is further supported by very sharp upper and lower boundaries of each unit, which indicate rapid deposition (and potentially erosion of loess material below). Colluvial palaeosols are not an uncommon feature in the loess landscape due to the erodibility of the material (Wolf and Faust, 2013), also supported by a heavily gullied and incised landscape in the vicinity of Slivata (Figure 2A). Finally the results of the zircon U-Pb age analysis point to larger contributions from Balkan Mountains at Slivata 2, and given the site's proximity to mountainous regions compared with other Lower Danube sites, the re-distribution of material from higher ground is likely (Figures 1 and 2). However, the genesis of these features cannot be resolved without further investigation using e.g. micromorphology, which could help to determine if pedogenic processes (e.g. clay coating, or biological activity) took place within sediment.

5.2.3. MIS 2

The investigated part of the Slivata 1 loess-palaeosol profile (Figure 4) covers the last ~23 ka and therefore preserves a record of the LGM. The stratigraphy varies from other loess profiles found in Romanian Plain e.g. Viatovo, Kaolinovo, Giurgiu (Balescu et al., 2020, 2018; Jordanova et al., 2007), mostly due to a thick LGM loess unit (over 5 m), which is more in line with the Lower Danube's Dobrogea sections, e.g. Urluia, Vlasca, Rasova, Balta Alba (Fitzsimmons and Hambach, 2014; Scheidt et al., 2021; Zeeden et al., 2018c). Figures 4, 7 and 10 show that the period between 23.5 and 20 ka at Slivata 1 is characterised higher preservation potential and/or higher availability of sediment, the highest proportion of sand (40%), U-ratio (3.7), and mean MARs (2413 g m^{-2} a^{-1}) all of which indicate a very dynamic aeolian environment, with strong gusty winds, an abundant sediment supply, and a relatively proximal source of the sediment. In contrast U-ratio, proportion of sand at sites in the Dobrogea region, Nosak, and Orlovat (Figure 10) and at most sites (apart from Surduk 2 and Rasova) MARs (Figure 7) are significantly lower than those recorded at Slivata 1, suggesting later peak in aeolian activity at Slivata. Whilst the Tăuşoare Cave shows a decrease in $\delta^{18}O$ values, the Black Sea lake temperature is initially relatively high, but it drops very dramatically albeit temporarily around 21 ka (Figure 10). That period coincides with the highest rates at Slivata 1 for both Lower and Middle Danube (Figure 7), suggesting that this region was experiencing drier conditions with more sediment available or that the higher MARs reflect an increased luminescence resolution. The pattern of high MARs followed by a drop and rise could potentially be linked to multiple larger glacial advance phases at ~21 ka, ~19.5 ka, and ~16.3 ka in the South Carpathians (Ruszkiczay-Rüdiger et al., 2016).

The thin palaeosol like horizons in Unit VI are likely to also represent colluvial deposits, as the units at Slivata 2 did, as the rate of pedogenesis is unlikely to exceed the rate of sediment delivery. However, the pedogenic horizon in Unit IV that developed between 20-19 ka corresponds to a drop in U-ratio and MARs (Figure 7), an increase in χfd, and plots mostly on top of the trendline (Figure 9A) suggesting pedogenic enhancement. Whilst this period represents the height of the LGM, a rise in $\delta^{18}O$ values in Tăuşoare Cave (Figure 10) and a temporary glacial retreat in South Carpathians have been suggested between 21-19.5 ka (Ruszkiczay-Rüdiger et al., 2016), indicating a brief period of environmental stability that could support enhanced pedogenic processes. Thin LGM age palaeosols are not specific to Slivata, as a high number of palaeosol like features developed between 25.0±2.1 ka and 16.3±1.3 ka in Stayky, Ukraine (Veres et al., 2018). These were interpreted as embryonic palaeosols previously thought to be driven by changes in the North Atlantic climate system (Rousseau et al., 2011). However, the site's continental position (and the likely blocking of the Atlantic influences by the Siberian High) and chronology presented by Veres et al. (2018) showed a lack of concurrence with Greenland ice core $\delta^{18}O$ isotope records, which record less variability for the period of 19.57±1.07 ka to 22.04±1.05 ka (Figure 10). Without further micromorphological analysis, for both Slivata or Stayky, it is not possible to conclude the genesis of these units, or to test whether they are linked to more localised hydroclimatic and/or environmental influences on palaeosol development rather than a regional pattern. The final loess bed (Unit II) is primarily silt size sediment, with a decrease in the U-ratio, and a drop in MARs to rates similar to those seen elsewhere along the Danube (Figure 7) and suggest a gradual shift from arid and windy glacial environment to interglacial conditions.

5.2.4. Holocene

The OSL age places the deposition of parent material for the Holocene soil shortly prior to 14.11±1.07 ka (modelled to boundary at 15.28 ka). The χfd increases only a little over this period, and samples plot very close to, albeit to the left of, the true loess line (Figure 9A). Therefore, Unit II is likely explained by the climatically driven magnetic enhancement, suggesting that favourable conditions for vegetation growth and soil processes to exceed the sediment supply rate might have occurred prior to Holocene onset at ~11.7 ka BP as suggested by Constantin et al. (2019). Chironomid records from the South Carpathians indicate a rapid summer temperature rise around ~14,700 cal BP, followed by a weakly expressed Younger Dryas cooling (Tóth et al., 2012), which are supported by the absence of geomorphological and chronological evidence associated glacial re-advance (Ruszkiczay-Rüdiger et al., 2016). The enhanced moisture delivery pre- and during Younger Dryas (Rea et al., 2020) likely translates to the observed glacial re-advance at ~13.5 ka in the South Carpathians (Ruszkiczay-Rüdiger et al., 2016), and at Slivata 1 pre-Holocene onset of pedogenesis.

5.3. A global or regional environmental and climatic record?

For global signals, loess-palaeosol profiles in a plateau-like setting are often preferentially investigated as it is argued that the stable depositional environment results in a preservation of global climatic and environmental influence correlations (Marković et al., 2018a). In turn the orbital scale drivers translate to a much less complex stratigraphy, aid inter-profile pedostratigraphic and proxy comparisons, and upscaling to develop regional loess stratigraphic models (Marković et al., 2016, 2015). Even though it could be argued that Slivata sits on small plateau-feature (Figure 2) dissected by the Lom and Skomlya rivers, the stratigraphic and sedimentological records show much higher complexity than one associated with plateau sites, such as Titel (Bokhorst et al., 2011; Marković et al., 2012; Perić et al., 2019). Nonetheless, as evidenced by the chronological results Slivata, preserves a near continuous record of the last glacial-interglacial cycle, and responds to global scale changes as evidenced by the stratigraphy, with extensive palaeosol associated with warmer periods and loess deposition during glacial periods.

Whilst Slivata preserves record of global scale changes, the results of the sedimentological, chronological and provenance analysis show that this site is strongly influenced by both microclimate and/or local environmental factors, such as palaeotopography, seasonality, proximity to the mountains, etc. This is particularly evidenced by the numerous palaeosols that do not conform to the typical orbital scale changes, e.g. Unit IV at Slivata 1 which developed between 20-19 ka. The intensity and speed of pedogenesis are site specific and depend on a number of factors that are not necessarily climatically driven. One of them being relief, resulting in palaeosol development and type that may not be spatially uniform or uninterrupted (Sauer et al., 2016; Vandenberghe et al., 2014b). In some cases these changes can be identified through sloping palaeosols, gullies, and shifts in the depositional environment (e.g. to fluvial) (Fenn et al., 2020a; Lehmkuhl et al., 2016; Vandenberghe et al., 2014b). However given the loess sediment homogeneity and that new sediment has the same properties as the previously deposited material, shifts may not be obvious even after sedimentary analysis and interpretation, and changes palaeotopography may be difficult to reconstruct. In the case of Slivata there are suggestions that the topography has been highly variable; evidenced by heavily incised gullies in the area and thick palaeosol, e.g. Unit II Slivata 2 (not discussed in detail in this study) that indicate development in a shallow gully or a channel. The sedimentological data from Slivata (Figures 4, 5 and 10) also show that while broad orbital scale trends match regional sedimentological changes observed across the Middle and Lower Danube, there are differences in the expression of the signal. In both U-ratio and χfd short lived abrupt shifts are preserved that do not fit with records such as Greenland (Figure 10). Instead these point to highly unstable conditions, and seasonal influences on the site. MARs (Figure 7) indicate that sediment accumulation and deposition is highly variable between sites over very short distances, further supporting the importance of local factors, such as topography, sediment availability, presence of vegetation, and local climatic conditions (e.g. wind direction and strength), in the development of loess profiles. At present we do not know what the main driver(s) of changes at Slivata is, it is encouraging that evidence of changes in regional and local conditions can be imprinted onto “the main” loess and palaeosol units, providing an opportunity to research smaller scale processes, and leads and lags between loess profiles (especially when it comes to dust fluxes). Whilst complex stratigraphies and sites might present many challenges in their interpretation, this research shows that there is a very rich palaeoenvironmental record preserved at these non-plateau sites.

6. Conclusion

This study provides the results of a high-resolution particle size, magnetic susceptibility investigation supported by 18 luminescence ages and zircon U-Pb ages for two loess profiles at Slivata, Bulgaria covering most of the last glacial cycle. The chronological framework is also enhanced by the identification of a tephra layer, geochemically correlated to Cape Riva (Y-2) tephra, which is the most northerly terrestrial detection of this volcanic ash. This has implications for both the loess and tephra communities, as the occurrence of Cape Riva (Y-2) in the Lower Danube loess provides a new tephrostratigraphic marker for directly linking loess sites with Mediterranean palaeoclimatic archives during the LGM.

The combination of the tephra marker and luminescence dating provides a robust basis for connecting both Slivata profiles and developing an age depth model. While the chronology encapsulates almost the whole glacial-interglacial cycle, the primary focus of the sedimentological work covers the last ~52 ka. The sedimentological, chronological, and provenance data presented suggests that Slivata was strongly affected by localised palaeotopographic and geomorphic factors which resulted in discrepancies between the stratigraphic records at both sites despite the short distance between them. The provenance data suggests that there was a minor switch in the sediment source/delivery mode in the transition between MIS 2 and MIS 3. This supports the interpretation of the palaeosol-like horizons as in-washed soil sediment, rather than pedogenic features, based on their timing of deposition, sedimentation rates and provenance signatures. The environmental reconstruction points to a very dynamic system with plenty of available sediment for deposition during the LGM and deglaciation.

Slivata profiles show differences between other Romanian and Bulgarian loess profiles, including the thickness of individual units, palaeosol development, and appearance of units. Therefore, while Slivata loess-palaeosol sequences preserve orbital scale climatic changes (i.e. glacial, interglacial) the record is overprinted by the regional hydrological and climatic factors, as well palaeotopography and geomorphology, which result in a more complex late Quaternary history. In particular, the modifying effect of the Carpathian Mountains is explored as similar features occur in the loess profile at Nosak on the other side of the Carpathian belt.

The results from Slivata demonstrate that sites away from a plateau setting and under the influence of a local climate can preserve in loess a much more detailed and complex record of palaeoclimatic changes than “cold and dry”.

Acknowledgements

This research was funded by the UK Natural Environmental Research Council (grant: NE/L002612/1), NIGL Natural Environmental Research Council grant, International Association of Sedimentologists Postgraduate Research Grants, and Hertford College Travel Fund. We are grateful to the two reviewers of this article for their time and comments, which have helped to improve the quality of this manuscript. Finally, the lead author would like to acknowledge the academic and mental support of WHWR during the COVID-19 pandemic.

7. References

Albani, S., Mahowald, N.M., Winckler, G., Anderson, R.F., Bradtmiller, L.I., Delmonte, B., François, R., Goman, M., Heavens, N.G., Hesse, P.P., Hovan, S.A., Kang, S., Kohfeld, K.E., Lu, H., Maggi, V., Mason, J.A., Mayewski, P.A., McGee, D., Miao, X., Otto-Bliesner, B.L., Perry, A.T., Pourmand, A., Roberts, H.M., Rosenbloom, N., Stevens, T., Sun, J., 2015. Twelve thousand years of dust: The Holocene global dust cycle constrained by natural archives. Clim. Past 11, 869–903. https://doi.org/10.5194/cp-11-869-2015

Andersen, T., Kristoffersen, M., Elburg, M.A., 2018. Visualizing, interpreting and comparing detrital zircon age and Hf isotope data in basin analysis – a graphical approach. Basin Res. 30, 132–147. https://doi.org/10.1111/bre.12245

Antoine, P., Catt, J.A., Lautridou, J.P., Sommé, J., 2003. The loess and coversands of northern France and southern England. J. Quat. Sci. 18, 309–318. https://doi.org/10.1002/jqs.750

Antoine, P., Lagroix, F., Jordanova, D., Jordanova, N., Lomax, J., Fuchs, M., Debret, M., Rousseau, D.-D., Hatté, C., Gauthier, C., Moine, O., Taylor, S.N., Till, J.L., Coutard, S., 2019. A remarkable Late Saalian (MIS 6) loess (dust) accumulation in the Lower Danube at Harletz (Bulgaria). Quat. Sci. Rev. 207, 80–100. https://doi.org/10.1016/j.quascirev.2019.01.005

Antoine, P., Rousseau, D.-D., Degeai, J.P., Moine, O., Lagroix, F., Kreutzer, S., Fuchs, M., Hatté, C., Gauthier, C., Svoboda, J., Lisá, L., 2013. High-resolution record of the environmental response to climatic variations during the Last Interglacial-Glacial cycle in Central Europe: The loess-palaeosol sequence of Dolní Věstonice (Czech Republic).

Quat. Sci. Rev. 67, 17–38. https://doi.org/10.1016/j.quascirev.2013.01.014

Antoine, P., Rousseau, D.-D., Fuchs, M., Hatté, C., Gauthier, C., Marković, S.B., Jovanović, M., Gaudenyi, T., Moine, O., Rossignol, J., 2009a. High-resolution record of the last climatic cycle in the southern Carpathian Basin (Surduk, Vojvodina, Serbia). Quat. Int. 198, 19–36. https://doi.org/10.1016/j.quaint.2008.12.008

Antoine, P., Rousseau, D.-D., Moine, O., Kunesch, S., Hatté, C., Lang, A., Tissoux, H., Zöller, L., 2009b. Rapid and cyclic aeolian deposition during the Last Glacial in European loess: a high-resolution record from Nussloch, Germany. Quat. Sci. Rev. 28, 2955–2973. https://doi.org/10.1016/j.quascirev.2009.08.001

Antoine, P., Rousseau, D.-D., Zöller, L., Lang, A., Munaut, A.V., Hatté, C., Fontugne, M., 2001. High-resolution record of the last interglacial-glacial cycle in the nussloch loess-palaeosol sequences, Upper Rhine Area, Germany. Quat. Int. 76–77, 211–229. https://doi.org/10.1016/S1040-6182(00)00104-X

Avram, A., Constantin, D., Veres, D., Kelemen, S., Obreht, I., Hambach, U., Timar-Gabor, A., Marković, S.B., 2020. Testing polymineral post-IR IRSL and quartz SAR-OSL protocols on Middle to Late Pleistocene loess at Batajnica , Serbia. Boreas. https://doi.org/10.1111/bor.12442

Avramov, V.I., Jordanova, D., Hoffmann, V., Roesler, W., 2006. The role of dust source area and pedogenesis in three loess-palaeosol sections from North Bulgaria: A mineral magnetic study. Stud. Geophys. Geod. 50, 259–282. https://doi.org/10.1007/s11200-006-0015-y

Balescu, S., Jordanova, D., Forget Brisson, L., Hardy, F., Huot, S., Lamothe, M., 2020. Luminescence chronology of the northeastern Bulgarian loess-paleosol sequences (Viatovo and Kaolinovo). Quat. Int. 552, 15–24. https://doi.org/10.1016/j.quaint.2019.04.020

Balescu, S., Lamothe, M., 1994. Comparison of TL and IRSL age estimates of feldspar coarse grains from waterlain sediments. Quat. Geochronol. 13, 437–444.

Balescu, S., Lamothe, M., Panaiotu, Cristina, Panaiotu, Cristian, 2010. IRSL chronology of eastern Romanian loess sequences. Quaternaire 21, 115–126.

Balescu, S., Tuffreau, A., Dobrescu, R., Auguste, P., Bahain, J.J., Lamothe, M., Petculescu, A., Shao, Q., 2018. New data on the chronology of Palaeolithic sites in loessic environments of northeastern and southeastern Romania (Eastern periphery of the Carpathian Mountains). Anthropol. 122, 87–110. https://doi.org/10.1016/j.anthro.2018.02.001

Baumgart, P., Hambach, U., Meszner, S., Faust, D., 2013. An environmental magnetic fingerprint of periglacial loess: Records of Late Pleistocene loess-palaeosol sequences from Eastern Germany. Quat. Int. 296, 82–93. https://doi.org/10.1016/j.quaint.2012.12.021

Bird, A.F., Stevens, T., Rittner, M., Vermeesch, P., Carter, A., Andò, S., Garzanti, E., Lu, H., Nie, J., Zeng, L., Zhang, H., Xu, Z., 2015. Quaternary dust source variation across the Chinese Loess Plateau. Palaeogeogr. Palaeoclimatol. Palaeoecol. 435, 254–264. https://doi.org/10.1016/j.palaeo.2015.06.024

Blaauw, M., Christeny, J.A., 2011. Flexible paleoclimate age-depth models using an autoregressive gamma process. Bayesian Anal. 6, 457–474. https://doi.org/10.1214/11-BA618

Blockley, S.P.E., Lane, C.S., Hardiman, M., Rasmussen, S.O., Seierstad, I.K., Steffensen, J.P., Svensson, A.M., Lotter, A.F., Turney, C.S.M., Ramsey, C.B., 2012. Synchronisation of palaeoenvironmental records over the last 60,000 years, and an extended INTIMATE1event stratigraphy to 48,000 b2k. Quat. Sci. Rev. 36, 2–10. https://doi.org/10.1016/j.quascirev.2011.09.017

Blockley, S.P.E., Pyne-O'Donnell, S.D.F., Lowe, J.J., Matthews, I.P., Stone, A., Turney, C.S.M., Pollard, A.M., Molyneux, E.G., 2005. A new and less destructive laboratory procedure for the physical separation of distal glass tephra shards from sediments. Quat. Sci. Rev. 24, 1952–1960. https://doi.org/10.1016/j.quascirev.2004.12.008

Boengiu, S., Avram, S., Vladut, A., 2011. Perspectives in the analysis of the terraces of the Danube within the Oltenia Plain (Romania). Analele Univ. din Oradea - Ser. Geogr. 181–191.

Bokhorst, M.P., Vandenberghe, J., Sümegi, P., Łanczont, M., Gerasimenko, N.P., Matviishina, Z.N., Marković, S.B., Frechen, M., 2011. Atmospheric circulation patterns in central and eastern Europe during the Weichselian Pleniglacial inferred from loess grain-size records. Quat. Int. 234, 62–74. https://doi.org/10.1016/j.quaint.2010.07.018

Bösken, J., Klasen, N., Zeeden, C., Obreht, I., Marković, S.B., Hambach, U., Lehmkuhl, F., 2017. New luminescence-based geochronology framing the last two glacial cycles at the southern limit of European Pleistocene loess in Stalać (Serbia). Geochronometria 44, 150–161. https://doi.org/10.1515/geochr-2015-0062

Bøtter-Jensen, L., Bulur, E., Duller, G.A.T., Murray, A.S., 2000. Advances in luminescence instrument systems. Radiat. Meas. 32, 523–528. https://doi.org/10.1016/S1350-4487(00)00039-1

Brennan, B.J., Lyons, R.G., Phillips, S.W., 1991. Attenuation of alpha particle track dose for spherical grains. Int. J. Radiat. Appl. Instrumentation. Part 18, 249–253. https://doi.org/10.1016/1359-0189(91)90119-3

Bronk Ramsey, C., 1995. Radiocarbon calibration and analysis of stratigraphy: the OxCal program. Radiocarbon 37, 425–430. https://doi.org/10.1017/s0033822200030903

Buggle, B., Glaser, B., Zöller, L., Hambach, U., Marković, S.B., Glaser, I., Gerasimenko, N.P., 2008. Geochemical characterization and origin of Southeastern and Eastern European loesses (Serbia, Romania, Ukraine). Quat. Sci. Rev. 27, 1058–1075. https://doi.org/10.1016/j.quascirev.2008.01.018

Buggle, B., Hambach, U., Glaser, B., Gerasimenko, N.P., Marković, S.B., Glaser, I., Zöller, L., 2009. Stratigraphy, and spatial and temporal paleoclimatic trends in Southeastern/Eastern European loess–paleosol sequences. Quat. Int. 196, 86–106. https://doi.org/10.1016/j.quaint.2008.07.013

Buggle, B., Hambach, U., Müller, K., Zöller, L., Marković, S.B., Glaser, B., 2014. Iron mineralogical proxies and quaternary climate change in SE-European loess-paleosol sequences. Catena 117, 4–22. https://doi.org/10.1016/j.catena.2013.06.012

Cohen, J., Saito, K., Entekhabi, D., 2001. The role of the Siberian High in Northern Hemisphere climate variability. Geophys. Res. Lett. 28, 299–302. https://doi.org/10.1029/2000GL011927

Connor, S.E., Ross, S.A., Sobotkova, A., Herries, A.I.R., Mooney, S.D., Longford, C., Iliev, I., 2013. Environmental conditions in the SE Balkans since the Last Glacial Maximum and their influence on the spread of agriculture into Europe. Quat. Sci. Rev. 68, 200–215. https://doi.org/10.1016/j.quascirev.2013.02.011

Constantin, D., Begy, R.C., Vasiliniuc, S., Panaiotu, C., Necula, C., Codrea, V., Timar-Gabor, A., 2014. High-resolution OSL dating of the Costineşti section (Dobrogea, SE Romania) using fine and coarse quartz. Quat. Int. 334–335, 20–29. https://doi.org/10.1016/j.quaint.2013.06.016

Constantin, D., Veres, D., Panaiotu, C., Anechitei-Deacu, V., Groza, S.M., Begy, R.C., Kelemen, S., Buylaert, J.-P., Hambach, U., Marković, S.B., Gerasimenko, N.P., Timar-Gabor, A., 2019. Luminescence age constraints on the Pleistocene-Holocene transition recorded in loess sequences across SE Europe. Quat. Geochronol. 49, 71–77. https://doi.org/10.1016/j.quageo.2018.07.011

Druitt, T.H., 1985. Vent Evolution and Lag Breccia Formation during the Cape Riva Eruption of Santorini, Greece. J. Geol. 93, 439–454.

Duller, G.A.T., 2003. Distinguishing quartz and feldspar in single grain luminescence measurements. Radiat. Meas. 37, 161–165. https://doi.org/10.1016/S1350-4487(02)00170-1

Durcan, J.A., Duller, G.A.T., 2011. The fast ratio: A rapid measure for testing the dominance of the fast component in the initial OSL signal from quartz. Radiat. Meas. 46, 1065–1072. https://doi.org/10.1016/j.radmeas.2011.07.016

Durcan, J.A., King, G.E., Duller, G.A.T., 2015. DRAC: Dose Rate and Age Calculator for trapped charge dating. Quat. Geochronol. 28, 54–61. https://doi.org/10.1016/j.quageo.2015.03.012

Eastwood, W.J., Pearce, N.J.G., Westgate, J.A., Perkins, W.T., Lamb, H.F., Roberts, N.M.W., 1999. Geochemistry of Santorini tephra in lake sediments from Southwest Turkey. Glob. Planet. Change 21, 17–29. https://doi.org/10.1016/S0921-8181(99)00005-3

European Soils Bureau, N., 2005. Soil Atlas of Europe. European Commision, Luxembourg.

Evlogiev, J., 2015. Environment Impact Assessment Report on Investment Proposal “Construction of National Disposal Facility for Low and Intermediate Level Radioactive Waste e Ndf.” Sofia.

Evlogiev, J., 2007. Evidence for the Aeolian Origin of Loess in the Danubian Plain. Geol. Balc. 36, 31–39.

Evlogiev, J., 2000. The Quaternary in Northeast Bulgaria. Rev. Bulg. Geol. Soc. 61, 3–25.

Federman, A.N., Carey, S.N., 1980. Electron microprobe correlation of tephra layers from Eastern Mediterranean abyssal sediments and the Island of Santorini. Quat. Res. 13, 160–171. https://doi.org/10.1016/0033-5894(80)90026-5

Fenn, K., 2019. Provenance of late Quaternary loess along the Middle and Lower Danube River, Europe. Unpublished PhD thesis, University of Oxford.

Fenn, K., Durcan, J.A., Thomas, D.S.G., Banak, A., 2020a. A 180 ka record of environmental change at Erdut (Croatia): a new chronology for the loess–palaeosol sequence and its implications for environmental interpretation. J. Quat. Sci. 35, 582–593. https://doi.org/10.1002/jqs.3201

Fenn, K., Durcan, J.A., Thomas, D.S.G., Millar, I.L., Marković, S.B., 2020b. Re-analysis of late Quaternary dust mass accumulation rates in Serbia using new luminescence chronology for loess–palaeosol sequence at Surduk. Boreas 49, 634–652. https://doi.org/10.1111/bor.12445

Fenn, K., Prud'Homme, C., 2020. Dust Deposits: Loess, in: Reference Module in Earth Systems and Environmental Sciences. Elsevier, pp. 1–46. https://doi.org/10.1016/B978-0-12-818234-5.00028-6

Fenn, K., Stevens, T., Bird, A.F., Limonta, M., Rittner, M., Vermeesch, P., Andò, S., Garzanti, E., Lu, H., Zhang, H., Lin, Z., 2018. Insights into the provenance of the Chinese Loess Plateau from joint zircon U-Pb and garnet geochemical analysis of last glacial loess. Quat. Res. 89. https://doi.org/10.1017/qua.2017.86

Fitzsimmons, K.E., 2017. Reconstructing palaeoenvironments on desert margins: New perspectives from Eurasian loess and Australian dry lake shorelines. Quat. Sci. Rev. 171, 1–19. https://doi.org/10.1016/j.quascirev.2017.05.018

Fitzsimmons, K.E., Hambach, U., 2014. Loess accumulation during the last glacial maximum: Evidence from Urluia, southeastern Romania. Quat. Int. 334–335, 74–85. https://doi.org/10.1016/j.quaint.2013.08.005

Fitzsimmons, K.E., Marković, S.B., Hambach, U., 2012. Pleistocene environmental dynamics recorded in the loess of the middle and lower Danube basin. Quat. Sci. Rev. 41, 104–118. https://doi.org/10.1016/j.quascirev.2012.03.002

Fleitmann, D., Cheng, H., Badertscher, S., Edwards, R.L., Mudelsee, M., Göktürk, O.M., Fankhauser, A., Pickering, R., Raible, C.C., Matter, A., Kramers, J., Tüysüz, O., 2009. Timing and climatic impact of Greenland interstadials recorded in stalagmites from northern Turkey. Geophys. Res. Lett. 36, 1–5. https://doi.org/10.1029/2009GL040050

Forster, T., Evans, M.E., Heller, F., 1994. The frequency dependence of low field susceptibility in loess sediments. Geophys. J. Int. 118, 636–642. https://doi.org/10.1111/j.1365-246X.1994.tb03990.x

Fuchs, M., Rousseau, D.-D., Antoine, P., Hatté, C., Gauthier, C., Marković, S.B., Zöller, L., 2008. Chronology of the Last Climatic Cycle (Upper Pleistocene) of the Surduk loess sequence, Vojvodina, Serbia. Boreas 37, 66–73. https://doi.org/10.1111/j.1502-3885.2007.00012.x

Galbraith, R.F., Roberts, R.G., Laslett, G.M., Yoshida, H., Olley, J.M., 1999. Optical Dating of Single and Multiple Grains of Quartz From Jinmium Rock Shelter, Northern Australia: Part I, Experimental Design and Statistical Models. Archaeometry 41, 365–395. https://doi.org/10.1111/j.1475-4754.1999.tb00988.x

Gocke, M., Hambach, U., Eckmeier, E., Schwark, L., Zöller, L., Fuchs, M., Löscher, M., Wiesenberg, G.L.B., 2014. Introducing an improved multi-proxy approach for paleoenvironmental reconstruction of loess-paleosol archives applied on the Late

Pleistocene Nussloch sequence (SW Germany). Palaeogeogr. Palaeoclimatol. Palaeoecol. 410, 300–315. https://doi.org/10.1016/j.palaeo.2014.06.006

Guérin, G., Mercier, N., Adamiec, G., 2011. Dose-rate conversion factors: update. Anc. TL 29, 5–8.

Haesaerts, P., Damblon, F., Gerasimenko, N.P., Spagna, P., Pirson, S., 2016. The Late Pleistocene loess-palaeosol sequence of Middle Belgium. Quat. Int. 411, 25–43. https://doi.org/10.1016/j.quaint.2016.02.012

Hardiman, J.C., 2008. Deep sea tephra from Nisyros Island, eastern Aegean Sea, Greece. Geol. Soc. London, Spec. Publ. 161, 69–88. https://doi.org/10.1144/gsl.sp.1999.161.01.06

Haydoutov, I., 1989. Precambrian ophiolites, Cambrian island arc, and Variscan suture in the South Carpathian-Balkan region. Geology 17, 905–908. https://doi.org/10.1130/0091-7613(1989)017<0905:POCIAA>2.3.CO;2

Haydoutov, I., Yanev, S., 1997. The Protomoesian microcontinent of the Balkan Peninsula - A peri-Gondwanaland piece. Tectonophysics 272, 303–313. https://doi.org/10.1016/S0040-1951(96)00264-8

Hošek, J., Hambach, U., Lisá, L., Grygar, T.M., Horáček, I., Meszner, S., Knésl, I., 2015. An integrated rock-magnetic and geochemical approach to loess/paleosol sequences from Bohemia and Moravia (Czech Republic): Implications for the Upper Pleistocene paleoenvironment in central Europe. Palaeogeogr. Palaeoclimatol. Palaeoecol. 418, 344–358. https://doi.org/10.1016/j.palaeo.2014.11.024

Huntley, D.J., Baril, M.R., 1997. The K content of the K-feldspars being measured in optical dating or in thermoluminescence dating. Anc. TL 15, 11–13.

Jary, Z., Ciszek, D., 2013. Late Pleistocene loess-palaeosol sequences in Poland and western Ukraine. Quat. Int. 296, 37–50. https://doi.org/10.1016/j.quaint.2012.07.009

Jochum, K.P., Stoll, B., Herwig, K., Willbold, M., Hofmiann, A.W., Amini, M., Aarburg, S., Abouchami, W., Hellebrand, E., Mocek, B., Raczek, I., Stracke, A., Alard, O., Bouman, C., Becker, S., Dücking, M., Brätz, H., Klemd, R., De Bruin, D., Canil, D., Cornell, D., De Hoog, C.J., Dalpé, C., Danyushevshy, L., Eisenhauer, A., Gao, Y., Snow, J.E., Groschopf, N., Günther, D., Latkoczy, C., Guillong, M., Hauri, E.H., Höfer, H.E., Lahaye, Y., Horz, K., Jacob, D.E., Kasemann, S.A., Kent, A.J.R., Ludwig, T., Zack, T., Mason, P.R.D., Meixner, A., Rosner, M., Misawa, K., Nash, B.P., Pfänder, J., Premo, W.R., Sun, W.D., Tiepolo, M., Vannucci, R., Vennemann, T.W., Wayne, D., Woodhead, J.D., 2006. MPI-DING reference glasses for in situ microanalysis: New reference values for element concentrations and isotope ratios. Geochemistry, Geophys. Geosystems 7. https://doi.org/10.1029/2005GC001060

Jordanova, D., Hus, J., Geeraerts, R., 2007. Palaeoclimatic implications of the magnetic record from loess/palaeosol sequence Viatovo (NE Bulgaria). Geophys. J. Int. 171, 1036–1047. https://doi.org/10.1111/j.1365-246X.2007.03576.x

Karátson, D., Wulf, S., Veres, D., Magyari, E.K., Gertisser, R., Timar-Gabor, A., Novothny, Á., Telbisz, T., Szalai, Z., Anechitei-Deacu, V., Appelt, O., Bormann, M., Jánosi, C., Hubay, K., Schäbitz, F., 2016. The latest explosive eruptions of Ciomadul (Csomád) volcano, East Carpathians - A tephrostratigraphic approach for the 51-29 ka BP time interval. J. Volcanol. Geotherm. Res. 319, 29–51. https://doi.org/10.1016/j.jvolgeores.2016.03.005

Karkanas, P., White, D., Lane, C.S., Stringer, C., Davies, W., Cullen, V.L., Smith, V.C., Ntinou, M., Tsartsidou, G., Kyparissi-Apostolika, N., 2015. Tephra correlations and climatic events between the MIS6/5 transition and the beginning of MIS3 in Theopetra Cave, central Greece. Quat. Sci. Rev. 118, 170–181. https://doi.org/10.1016/j.quascirev.2014.05.027

Kehl, M., Vlaminck, S., Köhler, T., Laag, C., Rolf, C., Tsukamoto, S., Frechen, M., Sumita, M., Schmincke, H.U., Khormali, F., 2021. Pleistocene dynamics of dust accumulation and soil formation in the southern Caspian Lowlands - New insights from the loess-paleosol sequence at Neka-Abelou, northern Iran. Quat. Sci. Rev. 253. https://doi.org/10.1016/j.quascirev.2020.106774

Kohfeld, K.E., Harrison, S.P., 2003. Glacial-interglacial changes in dust deposition on the Chinese Loess Plateau. Quat. Sci. Rev. 22, 1859–1878. https://doi.org/10.1016/S0277-3791(03)00166-5

Kottek, M., Grieser, J., Beck, C., Rudolf, B., Rubel, F., 2006. World map of the Köppen-Geiger climate classification updated. Meteorol. Zeitschrift 15, 259–263. https://doi.org/10.1127/0941-2948/2006/0130

Kwiecien, O., Arz, H.W., Lamy, F., Wulf, S., Bahr, A., Röhl, U., Haug, G.H., 2008. Estimated reservoir ages of the Black Sea since the last glacial. Radiocarbon 50, 99–118. https://doi.org/10.1017/S0033822200043393

Lee, S., Ramsey, C.B., Hardiman, M., 2013. Modeling the Age of the Cape Riva (Y-2) Tephra. Radiocarbon 55, 741–747. https://doi.org/10.1017/s0033822200057891

Lehmkuhl, F., Nett, J., Pötter, S., Schulte, P., Sprafke, T., Jary, Z., Antoine, P., Wacha, L., Wolf, D., Zerboni, A., Hošek, J., Marković, S.B., Obreht, I., Sümegi, P., Veres, D., Zeeden, C., Boemke, B., Schaubert, V., Viehweger, J., Hambach, U., 2021. Loess landscapes of Europe – Mapping, geomorphology, and zonal differentiation. Earth-Science Rev. 215. https://doi.org/10.1016/j.earscirev.2020.103496

Lehmkuhl, F., Zens, J., Krauß, L., Schulte, P., Kels, H., 2016. Loess-paleosol sequences at the northern European loess belt in Germany: Distribution, geomorphology and stratigraphy. Quat. Sci. Rev. 153, 11–30. https://doi.org/10.1016/j.quascirev.2016.10.008

Lézine, A.M., von Grafenstein, U., Andersen, N., Belmecheri, S., Bordon, A., Caron, B., Cazet, J.P., Erlenkeuser, H., Fouache, E., Grenier, C., Huntsman-Mapila, P., Hureau-Mazaudier, D., Manelli, D., Mazaud, A., Robert, C., Sulpizio, R., Tiercelin, J.J., Zanchetta, G., Zeqollari, Z., 2010. Lake Ohrid, Albania, provides an exceptional multi-proxy record of environmental changes during the last glacial-interglacial cycle. Palaeogeogr. Palaeoclimatol. Palaeoecol. 287, 116–127. https://doi.org/10.1016/j.palaeo.2010.01.016

Licht, A., Pullen, A., Kapp, P., Abell, J., Giesler, N., 2016. Eolian cannibalism : Reworked loess and fluvial sediment as the main sources of the Chinese Loess Plateau. GSA Bull. 128, 944–956. https://doi.org/10.1130/B31375.1

Lomax, J., Fuchs, M., Antoine, P., Rousseau, D.-D., Lagroix, F., Hatté, C., Taylor, S.N., Till, J.L., Debret, M., Moine, O., Jordanova, D., 2018. A luminescence-based chronology for the Harletz loess sequence, Bulgaria. Boreas 48, 179–194. https://doi.org/10.1111/bor.12348

Longman, J., Veres, D., Ersek, V., Haliuc, A., Wennrich, V., 2019. Runoff events and related rainfall variability in the Southern Carpathians during the last 2000 years. Sci. Rep. 9, 1–14. https://doi.org/10.1038/s41598-019-41855-1

Maher, B.A., 2011. The magnetic properties of Quaternary aeolian dusts and sediments, and their palaeoclimatic significance. Aeolian Res. 3, 87–144. https://doi.org/10.1016/j.aeolia.2011.01.005

Mahowald, N.M., Muhs, D.R., Levis, S., Rasch, P.J., Yoshioka, M., Zender, C.S., Luo, C., 2006. Change in atmospheric mineral aerosols in response to climate: Last glacial period, preindustrial, modern, and doubled carbon dioxide climates. J. Geophys. Res. Atmos. 111, D10202. https://doi.org/10.1029/2005JD006653

Margari, V., Gibbard, P.L., Bryant, C.L., Tzedakis, P.C., 2009. Character of vegetational and environmental changes in southern Europe during the last glacial period; evidence from Lesvos Island, Greece. Quat. Sci. Rev. 28, 1317–1339.

https://doi.org/10.1016/j.quascirev.2009.01.008

Margari, V., Pyle, D.M., Bryant, C.L., Gibbard, P.L., 2007. Mediterranean tephra stratigraphy revisited: Results from a long terrestrial sequence on Lesvos Island, Greece. J. Volcanol. Geotherm. Res. 163, 34–54. https://doi.org/10.1016/j.jvolgeores.2007.02.002

Marković, S.B., Bokhorst, M.P., Vandenberghe, J., McCoy, W.D., Oches, E.A., Hambach, U., Gaudenyi, T., Jovanović, M., Zöller, L., Stevens, T., Machalett, B., 2008. Late Pleistocene loess-palaeosol sequences in the Vojvodina region, north Serbia. J. Quat. Sci. 23, 73–84. https://doi.org/10.1002/jqs

Marković, S.B., Fitzsimmons, K.E., Sprafke, T., Gavrilović, D., Smalley, I.J., Jović, V., Svirčev, Z., Gavrilov, M.B., Bešlin, M., 2016. The history of Danube loess research. Quat. Int. 399, 86–99. https://doi.org/10.1016/j.quaint.2015.09.071

Marković, S.B., Hambach, U., Catto, N., Jovanović, M., Buggle, B., Machalett, B., Zöller, L., Glaser, B., Frechen, M., 2009. Middle and Late Pleistocene loess sequences at Batajnica, Vojvodina, Serbia. Quat. Int. 198, 255–266. https://doi.org/10.1016/j.quaint.2008.12.004

Marković, S.B., Hambach, U., Stevens, T., Jovanović, M., O'Hara-Dhand, K., Basarin, B., Lu, H., Smalley, I.J., Buggle, B., Zech, M., Svirčev, Z., Sümegi, P., Milojković, N., Zöller, L., 2012. Loess in the Vojvodina region (Northern Serbia): An essential link between European and Asian Pleistocene environments. Geol. en Mijnbouw/Netherlands J. Geosci. 91, 173–188. https://doi.org/10.1017/S0016774600001578

Marković, S.B., Korač, M., Mrđič, N., Buylaert, J.-P., Thiel, C., McLaren, S.J., Stevens, T., Tomič, N., Petič, N., Jovanovič, M., Vasiljević, D.A., Sümegi, P., Gavrilov, M.B., Obreht, I., 2014a. Palaeoenvironment and geoconservation of mammoths from the Nosak loess–palaeosol sequence (Drmno, northeastern Serbia): Initial results and perspectives. Quat. Int. 334–335, 30–39. https://doi.org/10.1016/j.quaint.2013.05.047

Marković, S.B., Oches, E.A., McCoy, W.D., Frechen, M., Gaudenyi, T., 2007. Malacological and sedimentological evidence for "warm" glacial climate from the Irig loess sequence, Vojvodina, Serbia. Geochemistry, Geophys. Geosystems 8, 1–12. https://doi.org/10.1029/2006GC001565

Marković, S.B., Stevens, T., Kukla, G.J., Hambach, U., Fitzsimmons, K.E., Gibbard, P.L., Buggle, B., Zech, M., Guo, Z., Hao, Q., Wu, H., O'Hara-Dhand, K., Smalley, I.J., Újvári, G., Sümegi, P., Timar-Gabor, A., Veres, D., Sirocko, F., Vasiljević, D.A., Jary, Z., Svensson, A.M., Jović, V., Lehmkuhl, F., Kovács, J.I., Svirčev, Z., 2015. Danube loess stratigraphy - Towards a pan-European loess stratigraphic model. Earth-Science Rev.

148, 228–258. https://doi.org/10.1016/j.earscirev.2015.06.005

Marković, S.B., Stevens, T., Mason, J.A., Vandenberghe, J., Yang, S., Veres, D., Újvári, G., Timar-Gabor, A., Zeeden, C., Guo, Z., Hao, Q., Obreht, I., Hambach, U., Wu, H., Gavrilov, M.B., Rolf, C., Tomić, N., Lehmkuhl, F., 2018a. Loess correlations – Between myth and reality. Palaeogeogr. Palaeoclimatol. Palaeoecol. 509, 4–23. https://doi.org/10.1016/j.palaeo.2018.04.018

Marković, S.B., Sümegi, P., Stevens, T., Schaetzl, R.J., Obreht, I., Chu, W., Buggle, B., Zech, M., Zech, R., Zeeden, C., Gavrilov, M.B., Perić, Z., Svirčev, Z., Lehmkuhl, F., 2018b. The Crvenka loess-paleosol sequence: A record of continuous grassland domination in the southern Carpathian Basin during the Late Pleistocene. Palaeogeogr. Palaeoclimatol. Palaeoecol. 509, 33–46. https://doi.org/10.1016/j.palaeo.2018.03.019

Marković, S.B., Timar-Gabor, A., Stevens, T., Hambach, U., Popov, D., Tomić, N., Obreht, I., Jovanović, M., Lehmkuhl, F., Kels, H., Marković, R., Gavrilov, M.B., 2014b. Environmental dynamics and luminescence chronology from the Orlovat loess-palaeosol sequence (Vojvodina, northern Serbia). J. Quat. Sci. 29, 189–199. https://doi.org/10.1002/jqs.2693

Mejdahl, V., 1979. Thermoluminescence dating: Beta-dose attenuation in quartz grains. Archaeometry 21, 61–72.

Meszner, S., Kreutzer, S., Fuchs, M., Faust, D., 2013. Late Pleistocene landscape dynamics in Saxony, Germany: Paleoenvironmental reconstruction using loess-paleosol sequences. Quat. Int. 296, 94–107. https://doi.org/10.1016/j.quaint.2012.12.040

Moine, O., Antoine, P., Hatté, C., Landais, A., Mathieu, J., Prud’homme, C., Rousseau, D.-D., 2017. The impact of Last Glacial climate variability in west-European loess revealed by radiocarbon dating of fossil earthworm granules. Proc. Natl. Acad. Sci. 114, 6209–6214. https://doi.org/10.1073/pnas.1614751114

Muhs, D.R., 2013. The geologic records of dust in the Quaternary. Aeolian Res. 9, 3–48. https://doi.org/10.1016/j.aeolia.2012.08.001

Müller, U.C., Pross, J., Tzedakis, P.C., Gamble, C., Kotthoff, U., Schmiedl, G., Wulf, S., Christanis, K., 2011. The role of climate in the spread of modern humans into Europe. Quat. Sci. Rev. 30, 273–279. https://doi.org/10.1016/j.quascirev.2010.11.016

Murray, A.S., Schmidt, E.D., Stevens, T., Buylaert, J.-P., Marković, S.B., Tsukamoto, S., Frechen, M., 2014. Dating middle pleistocene loess from Stari Slankamen (Vojvodina, Serbia) - limitations imposed by the saturation behaviour of an elevated temperature IRSL signal. Catena 117, 34–42. https://doi.org/10.1016/j.catena.2013.06.029

Murray, A.S., Wintle, A.G., 2000. Luminescence dating of quartz using an improved single-aliquot regenerative-dose protocol. Radiat. Meas. 32, 57–73. https://doi.org/10.1016/S1350-4487(99)00253-X

Nie, J., Stevens, T., Rittner, M., Stockli, D.F., Garzanti, E., Limonta, M., Vermeesch, P., Saylor, J.E., Lu, H., Breecker, D., Hu, X., Bird, A.F., Ando, S., Liu, S., Resentini, A., Vezzoli, G., Peng, W., Carter, A., Ji, S., Pan, B., 2015. Loess Plateau storage of Northeastern Tibetan Plateau-derived Yellow River sediment. Nat. Commun. 6. https://doi.org/10.1038/ncomms9511

Novothny, Á., Frechen, M., Horváth, E., Wacha, L., Rolf, C., 2011. Investigating the penultimate and last glacial cycles of the Süttő loess section (Hungary) using luminescence dating, high-resolution grain size, and magnetic susceptibility data. Quat. Int. 234, 75–85. https://doi.org/10.1016/j.quaint.2010.08.002

Novothny, Á., Horváth, E., Frechen, M., 2002. The loess profile at Albertirsa, Hungary-Improvements in loess stratigraphy by luminescence dating. Quat. Int. 95–96, 155–163. https://doi.org/10.1016/S1040-6182(02)00036-8

Obreht, I., Hambach, U., Veres, D., Zeeden, C., Bösken, J., Stevens, T., Marković, S.B., Klasen, N., Brill, D., Burow, C., Lehmkuhl, F., 2017. Shift of large-scale atmospheric systems over Europe during late MIS 3 and implications for Modern Human dispersal. Sci. Rep. 7, 5848. https://doi.org/10.1038/s41598-017-06285-x

Obreht, I., Zeeden, C., Hambach, U., Veres, D., Marković, S.B., Bösken, J., Svirčev, Z., Bačević, N., Gavrilov, M.B., Lehmkuhl, F., 2016. Tracing the influence of Mediterranean climate on Southeastern Europe during the past 350,000 years. Sci. Rep. 6, 36334. https://doi.org/10.1038/srep36334

Obreht, I., Zeeden, C., Schulte, P., Hambach, U., Eckmeier, E., Timar-Gabor, A., Lehmkuhl, F., 2015. Aeolian dynamics at the Orlovat loess-paleosol sequence, northern Serbia, based on detailed textural and geochemical evidence. Aeolian Res. 18, 69–81. https://doi.org/10.1016/j.aeolia.2015.06.004

Pańczyk, M., Nawrocki, J., Bogucki, A.B., Gozhik, P., Łanczont, M., 2020. Possible sources and transport pathways of loess deposited in Poland and Ukraine from detrital zircon U-Pb age spectra. Aeolian Res. 45, A provenance study was carried out on loess deposi. https://doi.org/10.1016/j.aeolia.2020.100598

Paterne, M., Guichard, F., Duplessy, J.C., Siani, G., Sulpizio, R., Labeyrie, J., 2008. A 90,000-200,000 yrs marine tephra record of Italian volcanic activity in the Central Mediterranean Sea. J. Volcanol. Geotherm. Res. 177, 187–196.

https://doi.org/10.1016/j.jvolgeores.2007.11.028

Perić, Z., Lagerbäck Adolphi, E., Stevens, T., Újvári, G., Zeeden, C., Buylaert, J.-P., Marković, S.B., Hambach, U., Fischer, P., Schmidt, C., Schulte, P., Huayu, L., Shuangwen, Y., Lehmkuhl, F., Obreht, I., Veres, D., Thiel, C., Frechen, M., Jain, M., Vött, A., Zöller, L., Gavrilov, M.B., 2019. Quartz OSL dating of late quaternary Chinese and Serbian loess: A cross Eurasian comparison of dust mass accumulation rates. Quat. Int. 502, 30–44. https://doi.org/10.1016/j.quaint.2018.01.010

Perić, Z.M., Marković, S.B., Sipos, G., Gavrilov, M.B., Thiel, C., Zeeden, C., Murray, A.S., 2020. A post-IR IRSL chronology and dust mass accumulation rates of the Nosak loess-palaeosol sequence in northeastern Serbia. Boreas. https://doi.org/10.1111/bor.12459

Plissart, G., Diot, H., Monnier, C., Mârunţiu, M., Berger, J., 2012. Relationship between a syntectonic granitic intrusion and a shear zone in the Southern Carpathian-Balkan area (Almâj Mountains, Romania): Implications for late Variscan kinematics and Cherbelezu granitoid emplacement. J. Struct. Geol. 39, 83–102. https://doi.org/10.1016/j.jsg.2012.03.004

Prescott, J.R., Hutton, J.T., 1994. Cosmic ray contributions to dose rates for luminescence and ESR dating: Large depths and long-term time variations. Radiat. Meas. 23, 497–500. https://doi.org/10.1016/1350-4487(94)90086-8

Rea, B.R., Pellitero, R., Spagnolo, M., Hughes, P., Ivy-Ochs, S., Renssen, H., Ribolini, A., Bakke, J., Lukas, S., Braithwaite, R.J., 2020. Atmospheric circulation over Europe during the Younger Dryas. Sci. Adv. 6, 1–14. https://doi.org/10.1126/sciadv.aba4844

Rees-Jones, J., 1995. Optical dating of young sediments using fine-grain quartz. Anc. TL.

Rimbu, N., Lohmann, G., Ionita, M., 2014. Interannual to multidecadal Euro-Atlantic blocking variability during winter and its relationship with extreme low temperatures in Europe. J. Geophys. Res. Atmos. 119, 13621–13636. https://doi.org/10.1038/175238c0

Roeser, P.A., Franz, S.O., Litt, T., Ülgen, U.B., Hilgers, A., Wulf, S., Wennrich, V., Akçer ön, S., Viehberg, F.A., Çağatay, M.N., Melles, M., 2012. Lithostratigraphic and geochronological framework for the paleoenvironmental reconstruction of the last ~36 ka cal BP from a sediment record from Lake Iznik (NW Turkey). Quat. Int. 274, 73–87. https://doi.org/10.1016/j.quaint.2012.06.006

Rostek, F., Bard, E., 2013. Hydrological changes in eastern Europe during the last 40,000yr inferred from biomarkers in Black Sea sediments. Quat. Res. 80, 502–509. https://doi.org/10.1016/j.yqres.2013.07.003

Rousseau, D.-D., Antoine, P., Gerasimenko, N.P., Sima, A., Fuchs, M., Hatté, C., Moine, O., Zöller, L., 2011. North Atlantic abrupt climatic events of the last glacial period recorded in Ukrainian loess deposits. Clim. Past 7, 221–234. https://doi.org/10.5194/cp-7-221-2011

Rousseau, D.-D., Boers, N., Sima, A., Svensson, A.M., Bigler, M., Lagroix, F., Taylor, S.N., Antoine, P., 2017. (MIS3 & 2) millennial oscillations in Greenland dust and Eurasian aeolian records – A paleosol perspective. Quat. Sci. Rev. 169, 99–113. https://doi.org/10.1016/j.quascirev.2017.05.020

Ruszkiczay-Rüdiger, Z., Kern, Z., 2016. Permafrost or seasonal frost? A review of paleoclimate proxies of the last glacial cycle in the East Central European lowlands. Quat. Int. 415, 241–252. https://doi.org/10.1016/j.quaint.2015.07.027

Ruszkiczay-Rüdiger, Z., Kern, Z., Urdea, P., Braucher, R., Madarász, B., Schimmelpfennig, I., 2016. Revised deglaciation history of the Pietrele–Stânişoara glacial complex, Retezat Mts, Southern Carpathians, Romania. Quat. Int. 415, 216–229. https://doi.org/10.1016/j.quaint.2015.10.085

Satow, C., Tomlinson, E.L., Grant, K.M., Albert, P.G., Smith, V.C., Manning, C.J., Ottolini, L., Wulf, S., Rohling, E.J., Lowe, J.J., Blockley, S.P.E., Menzies, M.A., 2015. A new contribution to the Late Quaternary tephrostratigraphy of the Mediterranean: Aegean Sea core LC21. Quat. Sci. Rev. 117, 96–112. https://doi.org/10.1016/j.quascirev.2015.04.005

Sauer, D., Kadereit, A., Kühn, P., Kösel, M., Miller, C.E., Shinonaga, T., Kreutzer, S., Herrmann, L., Fleck, W., Starkovich, B.M., Stahr, K., 2016. The loess-palaeosol sequence of Datthausen, SW Germany: Characteristics, chronology, and implications for the use of the Lohne Soil as a marker soil. CATENA 146, 10–29. https://doi.org/10.1016/j.catena.2016.06.024

Savov, I., Ryan, J., Haydoutov, I., Schijf, J., 2001. Late Precambrian Balkan-Carpathian ophiolite — a slice of the Pan-African ocean crust?: geochemical and tectonic insights from the Tcherni Vrah and Deli Jovan massifs, Bulgaria and Serbia. J. Volcanol. Geotherm. Res. 110, 299–318. https://doi.org/10.1016/S0377-0273(01)00216-5

Schaetzl, R.J., Bettis, E.A., Crouvi, O., Fitzsimmons, K.E., Grimley, D.A., Hambach, U., Lehmkuhl, F., Marković, S.B., Mason, J.A., Owczarek, P., Roberts, H.M., Rousseau, D.-D., Stevens, T., Vandenberghe, J., Zárate, M.A., Veres, D., Yang, S., Zech, M., Conroy, J.L., Dave, A.K., Faust, D., Hao, Q., Obreht, I., Prud'Homme, C., Smalley, I.J., Tripaldi, A., Zeeden, C., Zech, R., 2018. Approaches and challenges to the study of loess -

Introduction to the LoessFest Special Issue. Quat. Res. 89, 563–618. https://doi.org/10.1017/qua.2018.15

Schaffernicht, E.J., Ludwig, P., Shao, Y., 2020. Linkage between dust cycle and loess of the Last Glacial Maximum in Europe. Atmos. Chem. Phys. 20, 4969–4986.

Schatz, A.-K., Buylaert, J.-P., Murray, A.S., Stevens, T., Scholten, T., 2012. Establishing a luminescence chronology for a palaeosol-loess profile at Tokaj (Hungary): A comparison of quartz OSL and polymineral IRSL signals. Quat. Geochronol. 10, 68–74. https://doi.org/10.1016/j.quageo.2012.02.018

Schatz, A.-K., Qi, Y., Siebel, W., Wu, J., Zöller, L., 2015. Tracking potential source areas of Central European loess: examples from Tokaj (HU), Nussloch (D) and Grub (AT). Open Geosci. 7, 678–720. https://doi.org/10.1515/geo-2015-0048

Schatz, A.-K., Zech, M., Buggle, B., Gulyás, S., Hambach, U., Marković, S.B., Sümegi, P., Scholten, T., 2011. The late Quaternary loess record of Tokaj, Hungary: Reconstructing palaeoenvironment, vegetation and climate using stable C and N isotopes and biomarkers. Quat. Int. 240, 52–61. https://doi.org/10.1016/j.quaint.2010.10.009

Scheidt, S., Berg, S., Hambach, U., Klasen, N., Pötter, S., Stolz, A., Veres, D., Zeeden, C., Brill, D., Brückner, H., Kusch, S., Laag, C., Lehmkuhl, F., Melles, M., Monnens, F., Oppermann, L., Rethemeyer, J., Nett, J.J., 2021. Chronological Assessment of the Balta Alba Kurgan Loess-Paleosol Section (Romania) – A Comparative Study on Different Dating Methods for a Robust and Precise Age Model. Front. Earth Sci. 8, 1–23. https://doi.org/10.3389/feart.2020.598448

Seymour, K.S., Christanis, K., Bouzinos, A., Papazisimou, S., Papatheodorou, G., Moran, E., Dénès, G., 2004. Tephrostratigraphy and tephrochronology in the Philippi peat basin, Macedonia, Northern Hellas (Greece). Quat. Int. 121, 53–65. https://doi.org/10.1016/j.quaint.2004.01.023

Shumilovskikh, L.S., Fleitmann, D., Nowaczyk, N.R., Behling, H., Marret, F., Wegwerth, A., Arz, H.W., 2014. Orbital- and millennial-scale environmental changes between 64 and 20 ka BP recorded in Black Sea sediments. Clim. Past 10, 939–954. https://doi.org/10.5194/cp-10-939-2014

Sima, A., Rousseau, D.-D., Kageyama, M., Ramstein, G., Schulz, M., Balkanski, Y., Antoine, P., Dulac, F., Hatté, C., 2009. Imprint of North-Atlantic abrupt climate changes on western European loess deposits as viewed in a dust emission model. Quat. Sci. Rev. 28, 2851–2866. https://doi.org/10.1016/j.quascirev.2009.07.016

Staubwasser, M., Drăguşin, V., Onac, B.P., Assonov, S., Ersek, V., Hoffmann, D.L., Veres, D., 2018. Impact of climate change on the transition of Neanderthals to modern humans in Europe. Proc. Natl. Acad. Sci. 115, 9116–9121. https://doi.org/10.1073/pnas.1808647115

Stevens, T., Adamiec, G., Bird, A.F., Lu, H., 2013. An abrupt shift in dust source on the Chinese Loess Plateau revealed through high sampling resolution OSL dating. Quat. Sci. Rev. 82, 121–132. https://doi.org/10.1016/j.quascirev.2013.10.014

Stevens, T., Buylaert, J.-P., Thiel, C., Újvári, G., Yi, S., Murray, A.S., Frechen, M., Lu, H., 2018. Ice-volume-forced erosion of the Chinese Loess Plateau global Quaternary stratotype site. Nat. Commun. 9, 983. https://doi.org/10.1038/s41467-018-03329-2

Stevens, T., Lu, H., Thomas, D.S.G., Armitage, S.J., 2008. Optical dating of abrupt shifts in the late Pleistocene East Asian monsoon. Geology 36, 415. https://doi.org/10.1130/G24524A.1

Stevens, T., Marković, S.B., Zech, M., Hambach, U., Sümegi, P., 2011. Dust deposition and climate in the Carpathian Basin over an independently dated last glacial–interglacial cycle. Quat. Sci. Rev. 30, 662–681. https://doi.org/10.1016/j.quascirev.2010.12.011

Stevens, T., Palk, C., Carter, A., Lu, H., Clift, P.D., 2010. Assessing the provenance of loess and desert sediments in northern China using U-Pb dating and morphology of detrital zircons. Geol. Soc. Am. Bull. 122, 1331–1344. https://doi.org/10.1130/B30102.1

Stevens, T., Sechi, D., Bradák, B., Orbe, R., Baykal, Y., Cossu, G., Tziavaras, C., Andreucci, S., Pascucci, V., 2020. Abrupt last glacial dust fall over southeast England associated with dynamics of the British-Irish ice sheet. Quat. Sci. Rev. 250. https://doi.org/10.1016/j.quascirev.2020.106641

Szelepcsényi, Z., Breuer, H., Sümegi, P., 2014. The climate of Carpathian Region in the 20th century based on the original and modified Holdridge life zone system. Cent. Eur. J. Geosci. 6, 293–307. https://doi.org/10.2478/s13533-012-0189-5

Terhorst, B., Kühn, P., Damm, B., Hambach, U., Meyer-Heintze, S., Sedov, S., 2014. Paleoenvironmental fluctuations as recorded in the loess-paleosol sequence of the Upper Paleolithic site Krems-Wachtberg. Quat. Int. 351, 67–82. https://doi.org/10.1016/j.quaint.2013.03.045

Terhorst, B., Sedov, S., Sprafke, T., Peticzka, R., Meyer-Heintze, S., Kühn, P., Solleiro Rebolledo, E., 2015. Austrian MIS 3/2 loess-palaeosol records-Key sites along a west-east transect. Palaeogeogr. Palaeoclimatol. Palaeoecol. 418, 43–56. https://doi.org/10.1016/j.palaeo.2014.10.020

Timar-Gabor, A., Vandenberghe, D.A.G., Vasiliniuc, S., Panaoitu, C.E., Panaiotu, C.G., Dimofte, D., Cosma, C., 2011. Optical dating of Romanian loess: A comparison between silt-sized and sand-sized quartz. Quat. Int. 240, 62–70. https://doi.org/10.1016/j.quaint.2010.10.007

Tomlinson, E.L., Smith, V.C., Albert, P.G., Aydar, E., Civetta, L., Cioni, R., Çubukçu, E., Gertisser, R., Isaia, R., Menzies, M.A., Orsi, G., Rosi, M., Zanchetta, G., 2015. The major and trace element glass compositions of the productive Mediterranean volcanic sources: Tools for correlating distal tephra layers in and around Europe. Quat. Sci. Rev. 118, 48–66. https://doi.org/10.1016/j.quascirev.2014.10.028

Tóth, M., Magyari, E.K., Brooks, S.J., Braun, M., Buczkó, K., Bálint, M., Heiri, O., 2012. A chironomid-based reconstruction of late glacial summer temperatures in the southern Carpathians (Romania). Quat. Res. 77, 122–131. https://doi.org/10.1016/j.yqres.2011.09.005

Újvári, G., Klötzli, U., 2015. U–Pb ages and Hf isotopic composition of zircons in Austrian last glacial loess: constraints on heavy mineral sources and sediment transport pathways. Int. J. Earth Sci. 104, 1365–1385. https://doi.org/10.1007/s00531-014-1139-x

Újvári, G., Klötzli, U., Kiraly, F., Ntaflos, T., 2013. Towards identifying the origin of metamorphic components in Austrian loess: insights from detrital rutile chemistry, thermometry and U–Pb geochronology. Quat. Sci. Rev. 75, 132–142. https://doi.org/10.1016/j.quascirev.2013.06.002

Újvári, G., Kovács, J.I., Varga, G., Raucsik, B., Marković, S.B., 2010. Dust flux estimates for the Last Glacial Period in East Central Europe based on terrestrial records of loess deposits: a review. Quat. Sci. Rev. 29, 3157–3166. https://doi.org/10.1016/j.quascirev.2010.07.005

Újvári, G., Molnár, M., Novothny, Á., Páll-Gergely, B., Kovács, J.I., Várhegyi, A., 2014a. AMS 14C and OSL/IRSL dating of the Dunaszekcső loess sequence (Hungary): Chronology for 20 to 150ka and implications for establishing reliable age-depth models for the last 40ka. Quat. Sci. Rev. 106, 140–154. https://doi.org/10.1016/j.quascirev.2014.06.009

Újvári, G., Stevens, T., Molnár, M., Demény, A., Lambert, F., Varga, G., Jull, A.J.T., Páll-Gergely, B., Buylaert, J.-P., Kovács, J.I., 2017. Coupled European and Greenland last glacial dust activity driven by North Atlantic climate. Proc. Natl. Acad. Sci. 201712651. https://doi.org/10.1073/pnas.1712651114

Újvári, G., Varga, A., Balogh-Brunstad, Z., 2008. Origin, weathering, and geochemical composition of loess in southwestern Hungary. Quat. Res. 69, 421–437. https://doi.org/10.1016/j.yqres.2008.02.001

Újvári, G., Varga, A., Ramos, F.C., Kovács, J.I., Németh, T., Stevens, T., 2012. Evaluating the use of clay mineralogy, Sr-Nd isotopes and zircon U-Pb ages in tracking dust provenance: An example from loess of the Carpathian Basin. Chem. Geol. 304–305, 83–96. https://doi.org/10.1016/j.chemgeo.2012.02.007

Újvári, G., Varga, A., Raucsik, B., Kovács, J.I., 2014b. The Paks loess-paleosol sequence: A record of chemical weathering and provenance for the last 800ka in the mid-Carpathian Basin. Quat. Int. 319, 22–37. https://doi.org/10.1016/j.quaint.2012.04.004

Ünal-İmer, E., Shulmeister, J., Zhao, J.-X., Tonguç Uysal, I., Feng, Y.-X., Duc Nguyen, A., Yüce, G., 2015. An 80 kyr-long continuous speleothem record from Dim Cave, SW Turkey with paleoclimatic implications for the Eastern Mediterranean. Sci. Rep. 5, 13560. https://doi.org/10.1038/srep13560

Vandenberghe, J., French, H.M., Gorbunov, A., Marchenko, S., Velichko, A.A., Jin, H., Cui, Z., Zhang, T., Wan, X., 2014a. The Last Permafrost Maximum (LPM) map of the Northern Hemisphere: Permafrost extent and mean annual air temperatures, 25-17ka BP. Boreas 43, 652–666. https://doi.org/10.1111/bor.12070

Vandenberghe, J., Marković, S.B., Jovanović, M., Hambach, U., 2014b. Site-specific variability of loess and palaeosols (Ruma, Vojvodina, northern Serbia). Quat. Int. 334–335, 86–93. https://doi.org/10.1016/j.quaint.2013.10.036

Vandenberghe, J., Nugteren, G., 2001. Rapid climatic changes recorded in loess successions. Glob. Planet. Change 28, 1–9. https://doi.org/10.1016/S0921-8181(00)00060-6

Vasiliniuc, S., Timar-Gabor, A., Vandenberghe, D.A.G., Panaiotu, C.G., Begy, R.C., Cosma, C., 2011. A high resolution optical dating study of the Mostiştea loess-palaeosol sequence (Se Romania) using sand-sized quartz. Geochronometria 38, 34–41. https://doi.org/10.2478/s13386-011-0007-8

Veres, D., Tecsa, V., Gerasimenko, N.P., Zeeden, C., Hambach, U., Timar-Gabor, A., 2018. Short-term soil formation events in last glacial east European loess, evidence from multi-method luminescence dating. Quat. Sci. Rev. 200, 34–51. https://doi.org/10.1016/J.QUASCIREV.2018.09.037

Vermeesch, P., 2018. IsoplotR: A free and open toolbox for geochronology. Geosci. Front. 9, 1479–1493. https://doi.org/10.1016/j.gsf.2018.04.001

Vermeesch, P., 2013. Multi-sample comparison of detrital age distributions. Chem. Geol. 341, 140–146. https://doi.org/10.1016/j.chemgeo.2013.01.010

Vermeesch, P., 2012. On the visualisation of detrital age distributions. Chem. Geol. 312–313, 190–194. https://doi.org/10.1016/j.chemgeo.2012.04.021

Vespa, M., Keller, J., Gertisser, R., 2006. Interplinian explosive activity of Santorini volcano (Greece) during the past 150,000 years. J. Volcanol. Geotherm. Res. 153, 262–286. https://doi.org/10.1016/j.jvolgeores.2005.12.009

Vinci, A., 1985. Distribution and chemical composition of tephra layers from Eastern Mediterranean abyssal sediments. Mar. Geol. 64, 143–155. https://doi.org/10.1016/0025-3227(85)90165-3

Vogel, H., Zanchetta, G., Sulpizio, R., Wagner, B., Nowaczyk, N.R., 2010. A tephrostratigraphic record for the last glacial–interglacial cycle from Lake Ohrid, Albania and Macedonia. J. Quat. Sci. 25, 320–338. https://doi.org/10.1002/jqs

Wacha, L., Frechen, M., 2011. The geochronology of the “Gorjanović loess section” in Vukovar, Croatia. Quat. Int. 240, 87–99. https://doi.org/10.1016/j.quaint.2011.04.010

Wegwerth, A., Ganopolski, A., Ménot, G., Kaiser, J., Dellwig, O., Bard, E., Lamy, F., Arz, H.W., 2015. Black Sea temperature response to glacial millennial-scale climate variability. Geophys. Res. Lett. 42, 8147–8154. https://doi.org/10.1002/2015GL065499

Wegwerth, A., Kaiser, J., Dellwig, O., Shumilovskikh, L.S., Nowaczyk, N.R., Arz, H.W., 2016. Northern hemisphere climate control on the environmental dynamics in the glacial Black Sea “Lake.” Quat. Sci. Rev. 135, 41–53. https://doi.org/10.1016/j.quascirev.2016.01.016

Wintle, A.G., Murray, A.S., 2006. A review of quartz optically stimulated luminescence characteristics and their relevance in single-aliquot regeneration dating protocols. Radiat. Meas. 41, 369–391. https://doi.org/10.1016/j.radmeas.2005.11.001

Wolf, D., Faust, D., 2013. Holocene sediment fluxes in a fragile loess landscape (Saxony, Germany). Catena 103, 87–102. https://doi.org/10.1016/j.catena.2011.05.011

Wolf, D., Kolb, T., Ryborz, K., Heinrich, S., Schäfer, I., Calvo, R., Sanchez, J., 2021. Evidence for strong relations between the upper Tagus loess formation (central Iberia) and the marine atmosphere off the Iberian margin during the last glacial period. Quat. Res. https://doi.org/10.1017/qua.2020.119

Wulf, S., Fedorowicz, S., Veres, D., Łanczont, M., Karátson, D., Gertisser, R., Bormann, M., Magyari, E.K., Appelt, O., Hambach, U., Gozhyk, P.F., 2016. The ‘Roxolany Tephra’

(Ukraine) − new evidence for an origin from Ciomadul volcano, East Carpathians. J. Quat. Sci. 31, 565–576. https://doi.org/10.1002/jqs.2879

Wulf, S., Kraml, M., Kuhn, T., Schwarz, M., Inthorn, M., Keller, J., Kuscu, I., Halbach, P., 2002. Marine tephra from the Cape Riva eruption (22 ka) of Santorini in the Sea of Marmara. Mar. Geol. 183, 131–141. https://doi.org/10.1016/S0025-3227(01)00302-4

Zech, R., Zech, M., Marković, S.B., Hambach, U., Huang, Y., 2013. Humid glacials, arid interglacials? Critical thoughts on pedogenesis and paleoclimate based on multi-proxy analyses of the loess-paleosol sequence Crvenka, Northern Serbia. Palaeogeogr. Palaeoclimatol. Palaeoecol. 387, 165–175. https://doi.org/10.1016/j.palaeo.2013.07.023

Zeeden, C., Dietze, M., Kreutzer, S., 2018a. Discriminating luminescence age uncertainty composition for a robust Bayesian modelling. Quat. Geochronol. 43, 30–39. https://doi.org/10.1016/j.quageo.2017.10.001

Zeeden, C., Hambach, U., Obreht, I., Hao, Q., Abels, H.A., Veres, D., Lehmkuhl, F., Gavrilov, M.B., Marković, S.B., 2018b. Patterns and timing of loess-paleosol transitions in Eurasia: Constraints for paleoclimate studies. Glob. Planet. Change 162, 1–7. https://doi.org/10.1016/j.gloplacha.2017.12.021

Zeeden, C., Hambach, U., Veres, D., Fitzsimmons, K.E., Obreht, I., Bösken, J., Lehmkuhl, F., 2018c. Millennial scale climate oscillations recorded in the Lower Danube loess over the last glacial period. Palaeogeogr. Palaeoclimatol. Palaeoecol. 509, 164–181. https://doi.org/10.1016/j.palaeo.2016.12.029

Zeeden, C., Kels, H., Hambach, U., Schulte, P., Protze, J., Eckmeier, E., Marković, S.B., Klasen, N., Lehmkuhl, F., 2016. Three climatic cycles recorded in a loess-palaeosol sequence at Semlac (Romania) – Implications for dust accumulation in south-eastern Europe. Quat. Sci. Rev. 154, 130–142. https://doi.org/10.1016/j.quascirev.2016.11.002